Experimental comparative study on thermal performance of latent heat storage tanks with pin, perforated, and rectangular fins at different orientations

Safari, Vahid; Kamkari, Babak; Hewitt, Neil; Hooman, Kamel

DOI
10.1016/j.tsep.2024.102401

Publication date
2024

Document Version
Final published version

Published in
Thermal Science and Engineering Progress

Thermal Science and Engineering Progress 48 (2024) 102401

Contents lists available at ScienceDirect

Thermal Science and Engineering Progress

journal homepage: www.sciencedirect.com/journal/thermal-science-and-engineering-progress

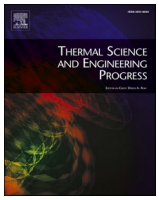

Experimental comparative study on thermal performance of latent heat storage tanks with pin, perforated, and rectangular fins at different orientations

Vahid Safari [a], Babak Kamkari [b,*], Neil Hewitt [c], Kamel Hooman [d]

[a] Department of Thermal and Fluids Engineering, Carlos III University of Madrid, Madrid, Spain
[b] School of Engineering, Ulster University, Belfast BT15 1AP, UK
[c] Centre for Sustainable Technologies, Belfast School of Architecture and the Built Environment, Ulster University, BT15 1AP, UK
[d] Process and Energy Department, Delft University of Technology, 2628 CB Delft, The Netherlands

ARTICLE INFO

Keywords:
Latent heat storage (LHS)
Phase change materials (PCM)
Melting
Heat transfer
Rectangular fin
Perforated fin
Pin fin

ABSTRACT

The low thermal conductivity of phase change materials (PCMs) has limited their widespread use in practical applications. In the present study, different fin structures, namely, rectangular, perforated, and pin were examined to analyze the thermal performance of the melting process in rectangular latent heat storage tanks. Experiments were performed at both horizontal and vertical orientations to evaluate the effectiveness of different fin configurations. Visual observation of the phase change evolution at different time intervals was enabled through a transparent plexiglass shell. Instantaneous heat transfer rate and energy storage were measured using thermocouple readings and melting photographs. The results show that the maximum heat transfer coefficient between the heated wall and PCM is obtained by the pin-finned tank followed by perforated and rectangular-finned tanks. This thermal behavior is justified by the intensification of the upward convection flows through the voids provided by pin fins or perforated fins. Although the rectangular fin structure has the lowest convective heat transfer coefficient, its heat transfer rate is slightly higher than the other structures due to its larger heat transfer area. At a wall temperature of 70℃, the convective heat transfer coefficient and heat transfer rate obtained by the pin fin configuration are respectively 25% higher and 4% less than those of the rectangular fin. It reveals that the pin fin structure provides the most effective heat transfer area compared to its counterparts which have a significantly larger fin volume. In addition, it was found that regardless of the fin configuration, the melting rate in the horizontal tank was significantly higher than in the vertical tank due to the formation of more vortical flow structures within the molten PCM. The melting time in the unfinned horizontal tank was less than those of the vertical finned tanks implying that the tank orientation should be well-chosen to minimize the melting time along with adding fins of various configurations.

1. Introduction

Over the past few years, energy consumption has dramatically increased in all residential, commercial, and industrial sectors. However, this increase in energy consumption has led to the depletion of fossil fuel resources and a significant rise in CO2 emissions. As a result, over 36 trillion tons of CO2 are emitted worldwide each year [1,2]. As a result, the global climate is expected to suffer an average temperature increase of 6 °C by 2050 [3]. Therefore, it is not surprising that significant emphasis has been placed on sustainable energy technologies. Renewable energy sources such as wind, solar, hydro, and biomass can help address these issues. Remarkable progress has been made in solar energy harvesting, and this energy source has been deemed one of the most promising [4]. Despite this, the main challenge with solar energy is its intermittent availability, i.e., the quantity of power generated by solar energy does not always meet the required amount. Recent studies have demonstrated that thermal energy storage (TES) can resolve the imbalance of solar energy supply/demand [5]. Thermal energy storage can be divided into sensible heat storage (SHS), latent heat storage (LHS), and thermochemical energy storage (TCES). Phase change materials (PCMs) with numerous solid to liquid and liquid to solid phase change cycles have been considered as one of the most prominent methods of thermal energy storage in recent decades due to their

* Corresponding author.
E-mail address: b.kamkari@ulster.ac.uk (B. Kamkari).

https://doi.org/10.1016/j.tsep.2024.102401
Received 17 September 2023; Received in revised form 20 December 2023; Accepted 10 January 2024
Available online 13 January 2024

Nomenclature

A	Heat transfer area (m^2)
C_p	Specific heat (kJ/kg.K)
h	Heat transfer coefficient ($W/m^2.K$)
h_{sl}	Latent heat of fusion (kJ/kg)
$< \overline{h} >$	Time-averaged heat transfer coefficient ($W/m^2.K$)
K	Thermal conductivity (W/m.K)
MF	Melt fraction
n	Number of thermocouples
N_p	Number of pixels
$Q_{sensible}$	Sensible stored thermal energy (kJ)
Q_{latent}	Latent stored thermal energy (kJ)
$< \overline{Q} >$	Time-averaged heat transfer rate (W)
t	Time (s)
T_{m1}	Onset of the melting process (℃)
T_{m2}	Endpoint of the melting process (℃)
T	Temperature (℃)
V	Volume (m^3)

Greek Symbols

ρ	Density (kg/m^3)
β	Solid to liquid volume expansion
δ	Uncertainty of the results

Subscripts

a	Apparent
CNC	Computer numerical control
EPDM	Ethylene propylene diene monomer
HTF	Heat transfer fluid
l	Liquid
m	Melting
MTR	Melting time reduction
PCM	Phase change material
r	Real
s	Solid
w	Wall
e	Enclosure
i	Initial

relatively large storage density and almost isothermal capacity [6]. Nevertheless, this system has one significant disadvantage: its low thermal conductivity, usually between 0.2 and 0.7 W/(m.K) [7]. A consequence of this drawback is the prolonged time required for charging and discharging. Thus, there is a need to enhance the thermal performance of the LHS systems [8]. There have been many techniques proposed for improving the performance of LHS systems, such as: using multiple PCMs [9,10], encapsulation of PCM [11], nanoparticles dispersion [12,13], metallic foam [14,15], and increasing the heat transfer surface between heat transfer fluid and PCM (fin) [16,17]. The latter technique has been the subject of numerous studies, and many researchers have explored the effects of extending surfaces in this context. Research has been conducted on fin configuration [18,19], number [20–22], thickness [23,24], length [25,26], and also fin material [27,28]. Additionally, the geometric design of thermal storage tanks plays an important role in determining the thermal performance of LHS systems [29]. Rectangular [30,31], sphere [32,33], and shell and tube units [34,35] are some of the geometries that have been studied the most. Liu et al. [36] conducted an experimental investigation regarding the effect of metal foam, pin-fins, and composite of them on PCM's melting process. The researchers concluded that a hybrid structure (incorporating fins and metal foam) reduces the melting time by 63.4 % compared to the unfinned storage tank. Using numerical optimization, Zhao et al. [37] determined the optimal fin structure inside a horizontal rectangular thermal storage tank. Fin material, height, and pitch were evaluated while fin volume remained constant at 5 %. The study found that there is an optimal fin pitch of 7.5 mm for a fin length of 25 mm. Further, they reported that the optimal fin length varies with the fin material, with a different trend for each material. Using lauric acid as a PCM, Karami and Kamkari [38] investigated the impact of solid and perforated fins on the thermal performance enhancement of shell and tube tanks. The results indicated that the tank with perforated fins reduces the melting time by 7 % compared to the tank with rectangular fins. Furthermore, they reported that the perforated fins provided more space for natural convection flows to ascend, resulting in a higher coefficient of convection heat transfer. Pakrouh et al. [39] performed a numerical analysis to determine the optimal geometry of a PCM-based heat sink comprising pin fins. The number, thickness, and height of fins were taken into consideration as geometric parameters. It has been reported that the optimum structure of fins always involves a pin fin with a longer height, but it is important to consider the critical temperature when determining the number and thickness of the fins. There have been similar findings reported by other researchers [40,41]. Safari et al. numerically [42] studied the melting behavior of PCM in one-side heated vertically and horizontally oriented rectangular thermal storage tanks under different fin numbers, lengths, and thicknesses. The results showed that longer fins could enhance the melting rate at the fixed number of fins due to providing a higher heat transfer area and boosting the thermal penetration depth. They reported that using a 9-fin horizontal tank with a fin length of 45 mm reduces the melting time by 75.1 % compared to a 3-fin vertical tank with a fin length of 25 mm (benchmark). Nakhchi and Esfahani [43] performed a numerical study regarding the effect of stepped fins on the melting rate improvement of a laterally-heated storage tank. They found that the downward-stepped fins are superior to the upward-stepped fins, and the melting time at the optimized downward-stepped fins is 65.5 % less than the conventional 3-fin storage tank.

To the best of our knowledge, there is a notable gap in existing research regarding a comprehensive comparative experimental study that investigates the effect of three specific types of fins (rectangular, perforated, and pin fins) on the melting rate of PCM in rectangular thermal storage tanks. While individual numerical or experimental studies may exist on each type of fin separately, there is a significant absence of a single comprehensive research study that thoroughly examines and compares the respective advantages and disadvantages of these fins. This study presents a pioneering experimental investigation into the impact of transitioning from traditional rectangular fins to perforated and pin fins in rectangular latent heat storage tanks, both vertically and horizontally. Perforated or pin fins are proposed as viable alternatives to conventional rectangular fins, offering the advantage of reducing the weight of the storage tank without significantly affecting the melting time. The findings highlight the importance of incorporating free space between fins to facilitate the development of natural convection in both vertical and horizontal directions. This work reveals the extent to which the heat transfer coefficient can be enhanced by using pin or perforated fins instead of rectangular fins. Furthermore, it has been found that simply reorienting vertical tanks horizontally can significantly improve melting rates rather than using fins of various configurations in a vertical orientation. By demonstrating the feasibility and benefits of using perforated and pin fins, this experimental study contributes to the advancement of thermal energy storage systems, providing valuable insights for designing more efficient and lightweight systems. Additionally, the results offer benchmarking data for validating numerical simulations.

2. Experimental setup and material properties

The photograph (a) and schematic (b) view of the fabricated experimental apparatus is illustrated in Fig. 1. The experimental setup comprises the following components: a thermal storage tank (1), thermocouples (2), a tilt-adjustable Table 3, a cold water bath (Advantec Toyo Kashia, model TBG045AA) (4), a hot water bath (Rigosha & Co., Japan) (5), a PID temperature controller (Rigosha & Co., Japan) (6), a personal computer (7), a temperature data acquisition system (Yokogawa, model DR-230) (8), a channel multiplexer (Yokogawa, model DS400) (9), and a circulation pump (Grundfos, model UPS 32–80) (10).

Lauric acid with a purity of 99 % (commonly known as dodecanoic acid), an environment-friendly fatty acid obtained from vegetable and animal oils, was used as a PCM inside the rectangular thermal storage tanks. Its desirable characteristics, such as non-toxicity, good chemical durability, and melting temperature range of 43℃-48℃, make it a suitable PCM for thermal energy storage applications at a medium temperature range. Thermal properties of lauric acid, such as phase change temperature, latent heat of fusion, and specific heat capacity determined by differential scanning calorimetry (DSC). The specific heat capacity (C_p) was calculated using the following equation:

$$C_p = \frac{dQ}{mdT} = \frac{\frac{dQ}{dt}}{m\frac{dT}{dt}} = \frac{\dot{Q}}{m\dot{T}} \tag{1}$$

In which, the heating and temperature change rates of the PCM with the specific mass (m) are denoted by $\dot{Q}$ and $\dot{T}$, respectively. Table 1 provides the values of these parameters, along with their corresponding accuracy, obtained during the DSC test.

Table 1
The characteristics for measuring the specific heat capacity of the PCM.

Spec	Unit	Value
PCM mass	(mg)	9.1 ± 0. 1
$\dot{T}\,(\frac{dT}{dt})$	(℃/min)	5 ± 0.2
$\dot{Q}_{liquidus}(\frac{dQ}{dt})$	(W)	$0.00189 \pm 7 \times 10^{-6}$
$\dot{Q}_{solidus}(\frac{dQ}{dt})$	(W)	$0.00183 \pm 7 \times 10^{-6}$

The latent heat of fusion (h_{sl}) was also determined by analyzing the DSC test data, and its value was calculated using the following equation:

$$h_{sl} = \frac{1}{m}\int_{t_1}^{t_2}\frac{dQ}{dt}dt = \sum_{i=1}^{i=n}\frac{\dot{Q}_i\Delta t}{m} \tag{2}$$

Table 2 presents the measured values of temperature and heat flow obtained during the melting process within the temperature range of 43.5 °C to 48.8 °C. These values were utilized in Eq. (2) to calculate the latent heat of fusion and to assess the associated uncertainty during the test.

More detailed information regarding the measurement of thermal properties of PCM can be found in the experimental research conducted by Shokouhmand [44]. A summary of the findings is presented in Table 3.

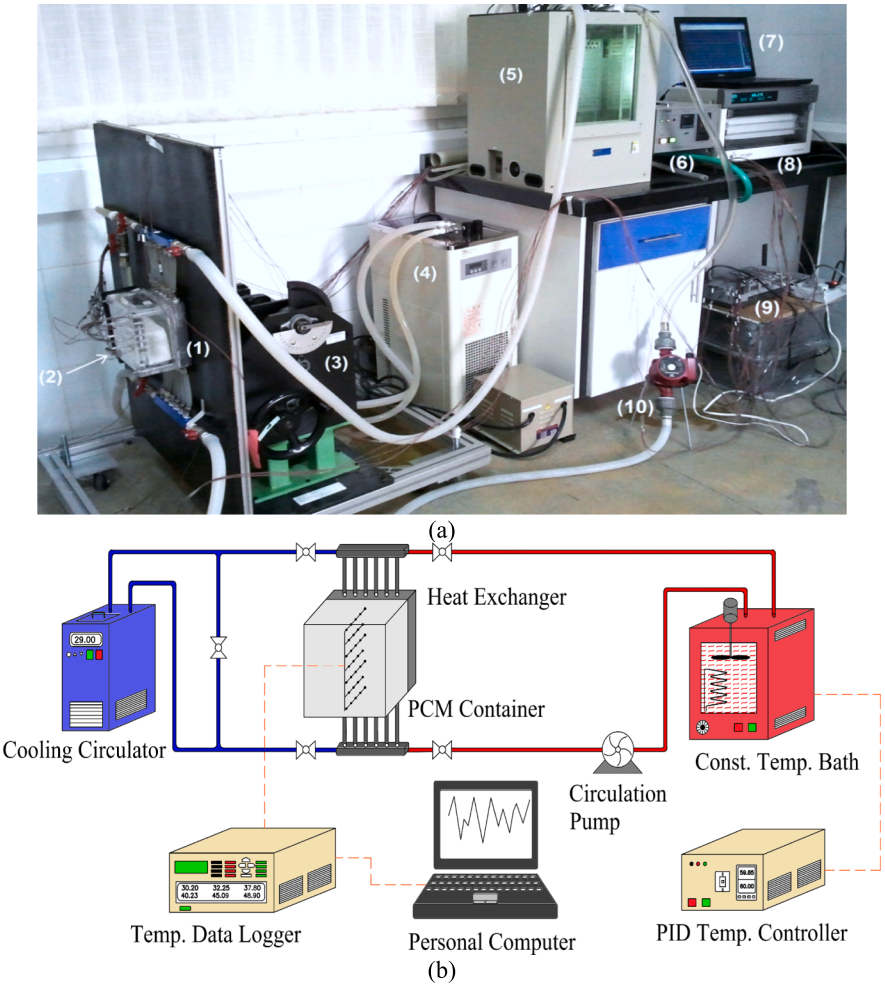

Fig. 1. The photograph (a) and schematic (b) view of the experimental setup.

Table 2
The measured values obtained during the DSC test for determining the..h_{sl}

Q (mW)	T (°C)	t (s)	Q (mW)	T (°C)	t (s)	Q (mW)	T (°C)	t (s)
43.78	45.55	442	35.45	44.22	423	5.79	43.50	404
40.63	45.73	443	37.29	44.25	424	6.53	43.56	405
38.36	45.88	444	39.11	44.28	425	7.39	43.62	406
36.57	46.01	445	40.91	44.31	426	8.56	43.67	407
34.77	46.15	446	42.71	44.34	427	9.86	43.72	408
32.71	46.29	447	44.45	44.37	428	11.25	43.76	409
30.60	46.44	448	46.12	44.41	429	12.70	43.80	410
28.63	46.58	449	47.79	44.44	430	14.25	43.84	411
26.66	46.72	450	49.46	44.48	431	15.85	43.88	412
24.48	46.86	451	51.02	44.51	432	17.53	43.91	413
21.63	47.03	452	52.35	44.56	433	19.26	43.94	414
18.98	47.19	453	53.48	44.61	434	21.00	43.98	415
16.48	47.35	454	53.72	44.68	435	22.73	44.01	416
13.94	47.51	455	53.85	44.76	436	24.48	44.04	417
11.35	47.67	456	53.67	44.85	437	26.25	44.07	418
9.04	47.82	457	53.00	44.95	438	28.08	44.10	419
7.20	47.95	458	52.03	45.06	439	29.94	44.13	420
5.68	48.08	459	49.90	45.21	440	31.78	44.16	421
			47.05	45.37	441	33.61	44.19	422

Table 3
Thermophysical properties of the lauric acid [44].

Specific heat capacity solid/liquid (kJ/kg K)	2.18/2.39
Melting temperature range (°C)	43.5/48.2
Latent heat of fusion (kJ/kg)	187.21
Thermal conductivity solid/liquid (W/m K)	0.16/0.14
Density solid/liquid (kg/m^3)	940/885
Kinematic viscosity (m^2/s)	6.7×10^{-6}

2.1. Fabricated storage tanks

The PCM tank is a rectangular enclosure with depth, width, and length of 5, 12, and 12 cm, respectively. For the heat transfer side, a 3.5 cm thick aluminum slab was drilled with six longitudinal holes for HTF circulation. It is worth mentioning that a HTF flow rate was maintained high enough to ensure a constant temperature distribution on the heat transfer surface. In order to monitor the temperature distribution, four thermocouples were mounted 2 mm below the surface, with two on each side of the heat exchanger. Throughout the experiments, a very uniform temperature distribution was observed on the heat transfer surface. Three different finned surfaces namely, rectangular fin, perforated fin, and pin fin have been made using CNC milling. The remaining five sides of the tank are made of transparent Plexiglas sheet with a thickness of 2.5 cm, allowing precise monitoring of the melting interface evolution and reducing heat loss from the tank due to its low thermal conductivity. EPDM sheets were used with a thickness of 3 cm to insulate the sidelong faces further. Fig. 2 shows the schematics of three different finned heat exchangers constructed to be compared with unfinned storage tanks. The geometrical dimensions were determined through a combination of literature review, theoretical considerations, and preliminary experiments. Commonly employed values were identified through a literature review, and the structural integrity requirements of the fins were considered. However, it is important to note that the current study represents an initial exploration, and further parametric studies are warranted. The determination of the optimal fin structure for each specific configuration is imperative and will be facilitated by these studies. By investigating various parameters, such as fin height, number, thickness, and spacing, a more refined understanding of the interplay between these factors and the heat transfer characteristics will be attained. The photograph of the fabricated finned storage tanks without a plexiglass shell can also be seen in Fig. 3.

Table. 4 presents the fin surface, volume, and PCM volume values for three fin structures and their variation compared to the rectangular fin configuration. The rectangular fin has the highest fin surface area and volume, followed by the perforated and pin fins. Interestingly, despite meaningful differences in fin surfaces, the amount of PCM in the tanks with rectangular and perforated fins is nearly equivalent. It is noteworthy that the fin volume can be significantly reduced by using pin fins instead of rectangular fins while the PCM volume remains very close to that of rectangular fins. It results in the construction of a tank that is both lighter and more economical.

2.2. Experimental procedure

Initially, solid PCM was heated to transform into liquid so it could be poured into the tanks. To avoid the formation of air pockets during the filling process, the liquid PCM was infused layer by layer into the storage tanks. Every liquid layer was about 1 cm in height. A sufficient amount of time should pass for the liquid layer to solidify, and then the next liquid layer can be infused into the solid layer below. The same procedure was repeated to fill the tanks with PCM completely. Due to the expansion of PCM during the solid–liquid phase change process, a space was left at the end side of the tank to receive the expanded liquid PCM. Fig. 4 illustrates the distribution of k-type thermocouples with a small diameter of 0.2 mm and a calibration accuracy of ±0.1 °C, located at the mid-plane of finned and unfinned enclosures (Fig. 5). In the unfinned and finned tanks, 32 and 26 thermocouples were installed, and temperatures were recorded every two seconds. To facilitate communication between the thermocouples and the data acquisition system, a channel multiplexer was employed. The multiplexer was used to connect all thermocouples. Subsequently, the data acquisition system was linked to the computer, and the DAQ32 software (Yokogawa, part of the Darwin series PC software) was utilized as the interface between the computer and the data acquisition system to record data at specific time intervals on the computer. A constant and uniform initial temperature distribution was ensured before each charging test by the circulation of cold water with a temperature of 24 °C through the drilled holes until all thermocouples reached the temperature of the inlet HTF. A charging test was initiated by passing the HTF with a fixed temperature from the thermal bath to the storage tanks. The process continued until a fully melted condition (no solid PCM) was reached. The melting interface was photographed every five minutes by removing the front face isolation. In order to examine the impact of HTF temperature on the melting process, three different HTF temperatures were chosen: 55, 60, and 70 °C. The charging experiments for the unfinned and rectangular-fin tanks were repeated three times at an inlet temperature of 60 °C to verify the reliability and repeatability of the tests. Perfect consistency between the temperature history and melt fraction results was observed.

3. Data reduction

3.1. Melt fraction

Melt fractions were calculated every 5 min from photographs taken during the phase change process. To determine the temporal melt fraction of the PCM, the MATLAB image processing toolbox was employed. Using contrast enhancement and filtering techniques, color photographs were turned into binary images. Binary images are composed of two-dimensional matrices comprising 0 and 1 elements, corresponding to black (liquid PCM) and white pixels (solid PCM), respectively. By dividing the number of pixels with 0 values by the total number of pixels in the binary image, one can calculate the apparent melt fraction as follow:

$$MF_a = \frac{N_{p_0}}{N_{p_t}} \tag{3}$$

Here, N_{p_0} represents the number of pixels with 0 values and N_{p_t} is the number of pixels in the binary image in total. It is necessary to include

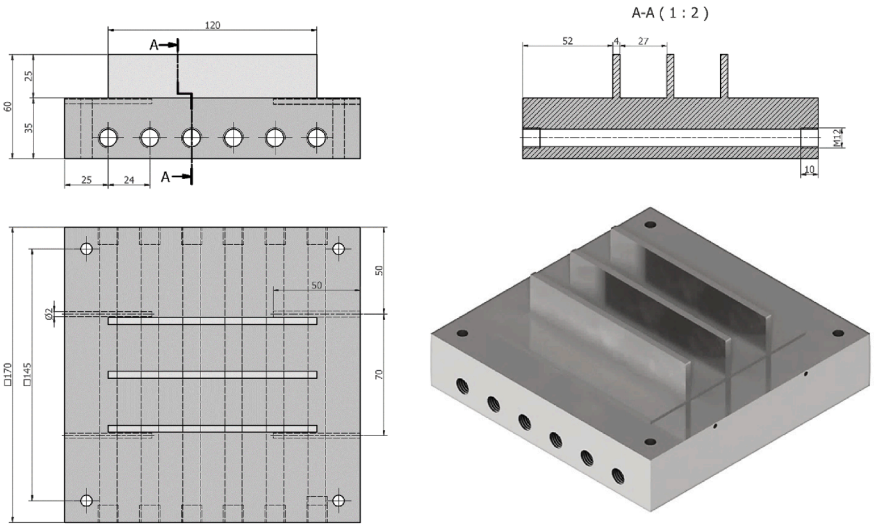

(a) Rectangular fin

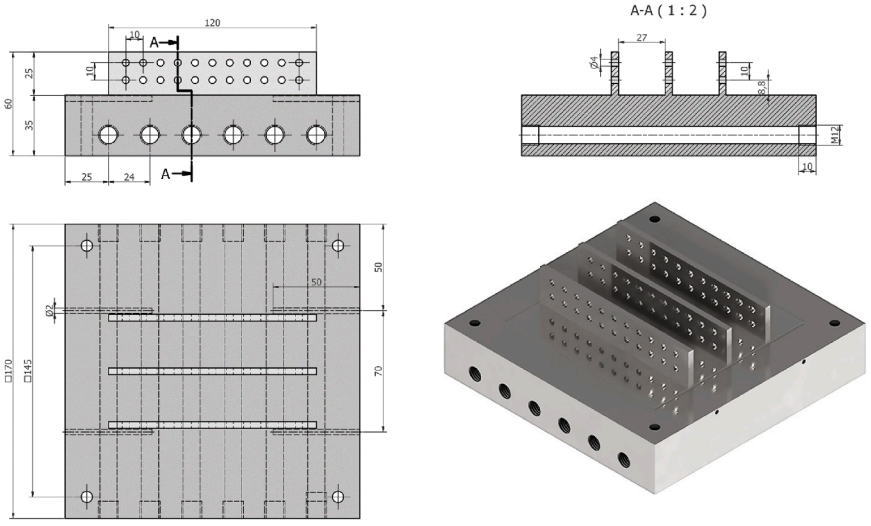

(b) Perforated fin

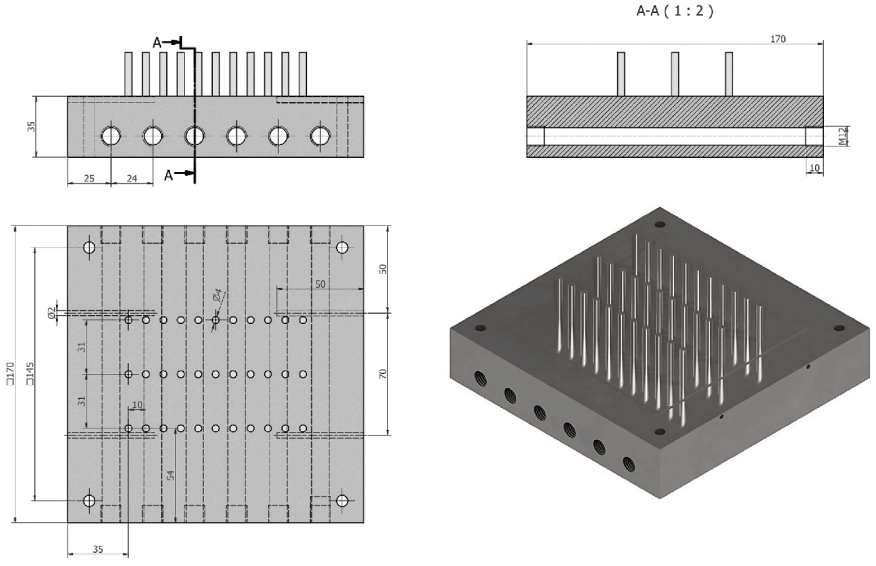

(c) Pin fin

Fig. 2. The schematics view of three different finned tanks with detailed specifications.

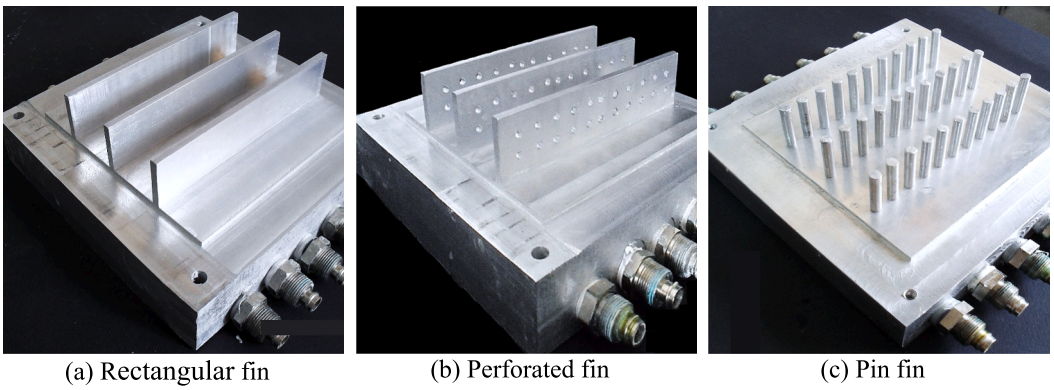

Fig. 3. The photograph of the fabricated storage tanks.

Table 4
Surface area and volume of the fins, along with PCM volume and mass for each case.

Fin type	Fin volume		Fin surface		PCM volume		PCM mass	
	Value (Cm^3)	Variation (%)	Value (Cm^2)	Variation (%)	Value (Cm^3)	Variation (%)	Value (g)	Variation (%)
Rectangular-fin	36	–	180	–	684	–	642.96	–
Perforated-fin	32.68	−9.22	163.42	−9.21	687.32	+0.48	646.08	+0.48
Pin-fin	10.36	−71.22	103.62	−42.43	709.64	+3.75	666.46	+3.75

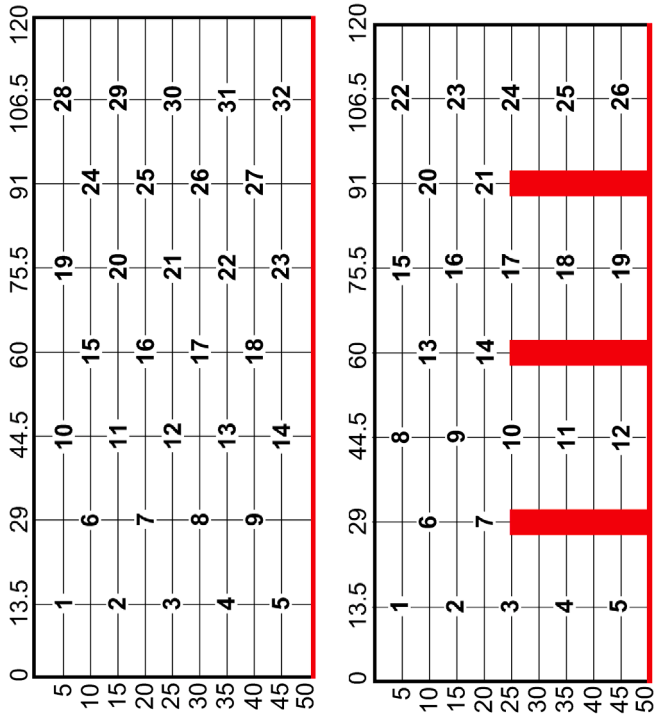

Fig. 4. The distribution of thermocouples inside the finned and unfinned tanks.

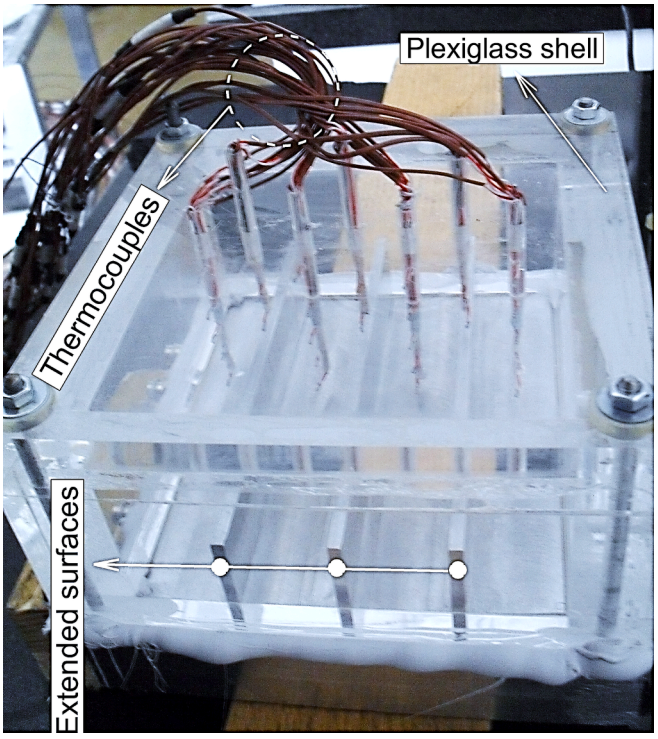

Fig. 5. The position of the thermocouples in depth direction of the tanks.

liquid drained from the tanks as a result of PCM expansion during the melting process. Therefore, Eq. (3) has been modified as follows:

$$MF_r = \frac{MF_a.(1+\beta)}{1+\beta.MF_a} \tag{4}$$

Where β represents the volume change from solid to liquid during the phase change process.

3.2. Energy storage

Based on the sensible and latent heat gained by PCM during the heat transfer process, the total thermal energy stored in the tanks can be calculated as follows:

$$Q_{total}(t) = Q_{sensible}(t) + Q_{latent}(t) \tag{5}$$

$$Q_{sensible}(t) = \int_{V_l(t)} \rho_s c_s (T_{m1} - T_i) dV_l + \int_{V_l(t)} \rho_l c_l \left(T_{mean_l}(t) - T_{m2}\right) dV_l + \int_{V_s(t)} \rho_s c_s (T_{mean_s}(t) - T_i) dV_s \quad (6)$$

$$Q_{latent}(t) = \rho_l M F_r(t) V_e (1 + \beta M F_a(t)) h_{sl} \quad (7)$$

In which, ρ and c denote the density and specific heat capacity for each phase (s for solid and l for liquid phase), respectively. T_{m1} and T_{m2} represent the onset and endpoint of the melting temperature range, while T_i signifies the initial temperature of the PCM. $T_{mean_s}(t)$ and $T_{mean_l}(t)$ are the instant average temperature of the solid and liquid phases, respectively, calculated using logged temperatures in the tanks as follows:

$$T_{mean_s}(t) = \frac{1}{n_s(t)} \sum_{k=1}^{n_s(t)} T_k \quad (8)$$

$$T_{mean_l}(t) = \frac{1}{n_l(t)} \sum_{k=1}^{n_l(t)} T_k \quad (9)$$

where $n_s(t)$ and $n_l(t)$ indicate the number of mounted thermocouples in solid and liquid PCM at each time interval, respectively. The constant β in Eq. (7), which accounts for the volume expansion during the solid-to-liquid phase change process, is calculated using the following equation.

$$\beta = \frac{V_l - V_s}{V_s} = \frac{\frac{V_l}{m} - \frac{V_s}{m}}{\frac{V_s}{m}} = \frac{\frac{1}{\rho_l} - \frac{1}{\rho_s}}{\frac{1}{\rho_s}} = \frac{\rho_s - \rho_l}{\rho_l} \quad (10)$$

3.3. Heat transfer rate and coefficient

Based on the absorbed energy by the PCM, the heat transfer rate between the heated wall and PCM during the time interwall of Δt can be calculated using the following relation:

$$\overline{Q}_{(t)} = \frac{Q_{total}(t + \Delta t) - Q_{total}(t)}{\Delta t} \quad (11)$$

In order to determine the time-average heat transfer rate during the entire melting process (t_{final}), the following formula can be used:

$$< \overline{Q} >= \frac{1}{t_{final}} \int_0^t \overline{Q}_{(t)} dt \quad (12)$$

The heat transfer coefficient on the surface of the isothermal wall during the time interwall of Δt can be obtained by:

$$\overline{h}_{(t)} = \frac{\overline{Q}_{(t)}}{A_w (T_w - T_m)} \quad (13)$$

where A_w is the total heat transfer area (isothermal wall and fins), and T_w and T_m represent the wall and melting temperature, respectively. The time-averaged heat transfer coefficient through the whole phase change process can be calculated as follows:

$$< \overline{h} >= \frac{1}{t_{final}} \int_0^t \overline{h}_{(t)} dt \quad (14)$$

3.4. Uncertainty analysis

The results of experiments are always subject to uncertainties associated with independent variables that were measured during the tests, which have an impact on how uncertainty propagates into the final results. According to Kline and McClintock approach [45], when the final result (R) is acquired from the independent variables of $x_1, x_2, \ldots, x_n$, the uncertainty of the result (δ_R) can be calculated as follows:

$$\delta_R = \sqrt{\sum_{i=1}^{n} \left(\frac{\partial y}{\partial x} \delta(x_i)\right)^2} \quad (15)$$

In which $\delta(x_i)$ represents the uncertainty of the independent variables. The uncertainty analysis for each variable is thoroughly explained in the subsequent section.

3.4.1. The uncertainty analysis for the specific heat capacity and latent heat of fusion

By applying the Kline and McClintock approach on Eq. (1) and (2), the uncertainty of the specific heat capacity and the latent heat of fusion can be expressed and calculated through the following equations:

$$\begin{aligned} \delta C_p &= \left[\left(\frac{\partial C_p}{\partial \dot{Q}} \delta \dot{Q}\right)^2 + \left(\frac{\partial C_p}{\partial m} \delta m\right)^2 + \left(\frac{\partial C_p}{\partial \dot{T}} \delta \dot{T}\right)^2 \right]^{\frac{1}{2}} \\ &= \left[\left(\frac{1}{m\dot{T}} \delta \dot{Q}\right)^2 + \left(\frac{\dot{Q}}{m^2 \dot{T}} \delta m\right)^2 + \left(\frac{\dot{Q}}{m\dot{T}^2} \delta \dot{T}\right)^2 \right]^{\frac{1}{2}} \end{aligned} \quad (16)$$

$$\begin{aligned} \delta h_{sl} &= \left[\left(\frac{\partial h_{sl}}{\partial \dot{Q}_1} \delta \dot{Q}_1\right)^2 + \left(\frac{\partial h_{sl}}{\partial \dot{Q}_2} \delta \dot{Q}_2\right)^2 + \cdots + \left(\frac{\partial h_{sl}}{\partial \dot{Q}_n} \delta \dot{Q}_n\right)^2 + \left(\frac{\partial h_{sl}}{\partial m} \delta m\right)^2 \right]^{\frac{1}{2}} \\ &= \left[\left(\frac{\Delta t}{m} \delta \dot{Q}_1\right)^2 + \left(\frac{\Delta t}{m} \delta \dot{Q}_2\right)^2 + \cdots + \left(\frac{\Delta t}{m} \delta \dot{Q}_n\right)^2 + \left(\frac{\dot{Q}_1 + \dot{Q}_2 + \cdots + \dot{Q}_n}{m^2} \Delta t \delta m\right)^2 \right]^{\frac{1}{2}} \end{aligned} \quad (17)$$

The maximum uncertainties of the specific heat capacity for the solid and liquid phases were calculated to be ±87.2 J/kg℃ and ±90.3 J/kg ℃, respectively. When expressed as percentages, these uncertainties are ±5.1 % and ±4.8 %, respectively. The maximum uncertainty for the latent heat of fusion was ±5650 J, corresponding to ±3.1 % when expressed as a percentage.

3.4.2. The uncertainty analysis of the PCM density, volume expansion and melt fraction

The density of the PCM was measured using a digital scale with an accuracy of ±1 mg, while the volume was determined using a graduated cylinder with an accuracy of ±1 ml. The uncertainty of the density in both the solid and liquid phases was calculated using the following equation:

$$\delta\rho = \left[\left(\frac{\partial\rho}{\partial m}\delta m\right)^2 + \left(\frac{\partial\rho}{\partial V}\delta V\right)^2\right]^{\frac{1}{2}} = \left[\left(\frac{1}{V}\delta m\right)^2 + \left(\frac{m}{V^2}\delta V\right)^2\right]^{\frac{1}{2}} \tag{18}$$

Using the Eq. (18), the maximum uncertainties for the solid and liquid phases were calculated as ±13.8 kg/m^3 and ±12.1 kg/m^3, respectively. The maximum uncertainty of the PCM volume expansion and melt fraction were also calculated through the following equations:

$$\delta\beta = \left[\left(\frac{\partial\beta}{\partial\rho_s}\delta\rho_s\right)^2 + \left(\frac{\partial\beta}{\partial\rho_l}\delta\rho_l\right)^2\right]^{\frac{1}{2}} = \left[\left(\frac{1}{\rho_l}\delta\rho_s\right)^2 + \left(\frac{\rho_s}{\rho_l{}^2}\delta\rho_l\right)^2\right]^{\frac{1}{2}} \tag{19}$$

$$\begin{aligned}\delta MF_r &= \left[\left(\frac{\partial MF_r}{\partial MF_\alpha}\delta MF_\alpha\right)^2 + \left(\frac{\partial MF_r}{\partial\beta}\delta\beta\right)^2\right]^{\frac{1}{2}} \\ &= \left[\left(\frac{1+\beta}{(1+\beta MF_\alpha)^2}\delta MF_\alpha\right)^2 + \left(\frac{MF_\alpha - MF_\alpha{}^2}{(1+\beta MF_\alpha)^2}\delta\beta\right)^2\right]^{\frac{1}{2}}\end{aligned} \tag{20}$$

It should be noted that in Eq. (20), the term δMF_α originates from the accuracy of pixel counting by MATLAB software and can be considered negligible. The maximum uncertainty value for the PCM volume expansion and melt fraction were found to be ±2.4 % and ±3.9 % respectively.

3.4.3. The uncertainty analysis of the stored energy, heat transfer rate and coefficient

The uncertainty of the stored sensible thermal energy can be determined as follows:

$$\delta Q_{sensible}(t) = \left[\begin{array}{c}\left(\frac{\partial Q_{sensible}(t)}{\partial\rho_s}\delta\rho_s\right)^2 + \left(\frac{\partial Q_{sensible}(t)}{\partial C_s}\delta C_s\right)^2 + \left(\frac{\partial Q_{sensible}(t)}{\partial T_{m1}}\delta T_{m1}\right)^2 + \\ \left(\frac{\partial Q_{sensible}(t)}{\partial T_i}\delta T_i\right)^2 + \left(\frac{\partial Q_{sensible}(t)}{\partial V_l}\delta V_l\right)^2 + \left(\frac{\partial Q_{sensible}(t)}{\partial\rho_l}\delta\rho_l\right)^2 + \\ \left(\frac{\partial Q_{sensible}(t)}{\partial C_l}\delta C_l\right)^2 + \left(\frac{\partial Q_{sensible}(t)}{\partial T_{mean_l}}\delta T_{mean_l}\right)^2 + \left(\frac{\partial Q_{sensible}(t)}{\partial T_{m2}}\delta T_{m2}\right)^2 + \\ \left(\frac{\partial Q_{sensible}(t)}{\partial T_{mean_s}}\delta T_{mean_s}\right)^2 + \left(\frac{\partial Q_{sensible}(t)}{\partial V_s}\delta V_s\right)^2\end{array}\right]^{\frac{1}{2}}$$

$$= \left[\begin{array}{c}((C_s\times(T_{m1}-T_i)\times V_l(t) + C_s\times(T_{mean_s}(t)-T_i)\times V_s(t))\times\delta\rho_s)^2 + \\ ((\rho_s(T_{m1}-T_i)V_l(t) + \rho_s(T_{mean_s}(t)-T_i)V_s(t))\times\delta C_s)^2 + \\ ((\rho_s C_s V_l(t))\times\delta T_{m1})^2 + ((\rho_s C_s V_l(t) + \rho_s C_s V_s(t))\times\delta T_i)^2 + \\ \left(\left(\rho_s C_s(T_{m1-}T_i) + \rho_l C_l(T_{mean_l}-T_{m2})\right)\times\delta V_l\right)^2 + \\ \left(\left(C_l(T_{mean_l}-T_{m2})V_l(t)\right)\times\delta\rho_l\right)^2 + \\ \left(\left(\rho_l(T_{mean_l}-T_{m2})V_l(t)\right)\times\delta C_l\right)^2 + \left(\left(\rho_l C_l V_l(t)\right)\times\delta T_{mean_l}\right)^2 \\ +((\rho_l C_l V_l(t))\times\delta T_{m2})^2 + \\ ((\rho_s C_s V_s(t))\times\delta T_{mean_s})^2 + ((\rho_s C_s(T_{mean_s}-T_i))\times\delta V_s)^2\end{array}\right]^{\frac{1}{2}} \tag{21}$$

In order to determine the uncertainty of the stored sensible heat, the uncertainty value of the average temperature is required, which can be calculated as follows:

$$\delta T_{mean_l} = \left[\left(\frac{1}{n_l(t)}\delta T_1\right)^2 + \left(\frac{1}{n_l(t)}\delta T_1\right)^2 + \ldots + \left(\frac{1}{n_l(t)}\delta T_n\right)^2\right]^{\frac{1}{2}} \tag{22}$$

The following equations were used to obtain the maximum uncertainty of the stored latent and total thermal energy.

$$\begin{aligned}\delta Q_{latent} &= \left[\left(\frac{\partial Q_{latent}}{\partial\rho_s}\delta\rho_s\right)^2 + \left(\frac{\partial Q_{latent}}{\partial MF(t))}\delta MF(t)\right)^2 + \left(\frac{\partial Q_{latent}}{\partial h_{sl}}\delta h_{sl}\right)^2\right]^{\frac{1}{2}} \\ &= \left[\begin{array}{c}(MF(t)\times V_e\times h_{sl}\times\delta\rho_s)^2 + (\rho_s\times V_e\times h_{sl}\times\delta MF(t))^2 + \\ (\rho_s\times\gamma(t)\times V_e\times\delta h_{sl})^2\end{array}\right]^{\frac{1}{2}}\end{aligned} \tag{23}$$

$$\begin{aligned}\delta Q_{total}(t) &= \left[\left(\frac{\partial Q_{total}(t)}{\partial Q_{sensible}(t)}\delta Q_{sensible}(t)\right)^2 + \left(\frac{\partial Q_{total}(t)}{\partial Q_{latent}(t)}\delta Q_{latent}(t)\right)^2\right]^{\frac{1}{2}} \\ &= \left[(\delta Q_{sensible}(t))^2 + (\delta Q_{latent}(t))^2\right]^{\frac{1}{2}}\end{aligned} \tag{24}$$

The uncertainty equations for the heat transfer rate and coefficient can also be expressed as:

$$\begin{aligned}\delta\overline{Q}_{(t)} &= \frac{1}{\Delta t}\times\left[\left(\frac{\partial\overline{Q}_{(t)}}{\partial Q_{total}(t+\Delta t)}\delta Q_{total}(t+\Delta t)\right)^2 - \left(\frac{\partial\overline{Q}_{(t)}}{\partial Q_{total}(t)}\delta Q_{total}(t)\right)^2\right]^{\frac{1}{2}} \\ &= \frac{1}{\Delta t}\times\left[(\delta Q_{total}(t+\Delta t))^2 + (\delta Q_{total}(t))^2\right]^{\frac{1}{2}}\end{aligned} \tag{25}$$

$$\begin{aligned}\delta\overline{h}_{(t)} &= \left[\left(\frac{\delta\overline{h}_{(t)}}{\partial\overline{Q}_{(t)}}\delta\overline{Q}_{(t)}\right)^2 + \left(\frac{\delta\overline{h}_{(t)}}{\partial A}\delta A\right)^2 + 2\times\left(\frac{\delta\overline{h}_{(t)}}{\partial T}\delta T\right)^2\right]^{\frac{1}{2}} \\ &= \left[\left(\frac{1}{A\times\Delta T}\partial\overline{Q}_{(t)}\right)^2 + \left(\frac{\overline{Q}_{(t)}}{A^2\times\Delta T}\delta A\right)^2 + 2\times\left(\frac{\overline{Q}_{(t)}}{A\times\Delta T}\delta T\right)^2\right]^{\frac{1}{2}}\end{aligned} \tag{26}$$

Based on the aforementioned equations, the maximum uncertainty values for the heat transfer rates, and coefficients were calculated to be ±8.4 %, and ±5.2 %, respectively.

4. Result and discussion

4.1. Temperature history

Temperature measurements at different points of the storage tanks provide valuable information regarding melting behavior, temperature distribution, and natural convection currents influenced by enclosure orientation and fin configuration. Fig. 6 presents the timewise temperature variation at different locations of unfinned enclosures with vertical (a) and horizontal (b) orientations at a wall temperature of 60 °C. Based on the recorded temperature histories, three distinct stages can be identified. Initially, heat is transferred from the hot surface to the solid PCM through the conduction mechanism. As a result, the temperature rises to the melting temperature range, during which the solid PCM absorbs sensible heat. After the PCM temperature reaches the phase change temperature (second stage), the melting process begins, and molten PCM passes through the tips of the thermocouples. This can be detected by the sharp increase in the temperature variation trend. During the final stage, liquid PCM receives sensible heat through the conduction mechanism and becomes superheated, during which the recorded temperature increases moderately. Fig. 6 (a) shows the temperature variation of the PCM in the vertical unfinned storage tank. At the beginning of the melting process, the temperature of the thermocouples placed in the same column increases in a similar trend. According to this temperature behavior, the PCM absorbs heat from a uniformly growing liquid layer parallel to the vertical hot layer, indicating that conduction is the predominant heat transfer mechanism. Once this short time passes, the temperatures of the thermocouples placed in a given column and upper rows exceed those in the lower rows. It is due to the formation of circulating convection currents that push the molten PCM upward, enhancing the heat transfer rate at the upper portion of the storage tank. Due to this, the upper portions of the tank experience a higher melting rate than the lower part. Considering the specific row of thermocouples, it can be seen that the steep increase in temperature occurs faster at the points closer to the isothermal surface, demonstrating the propagation direction of the thermal boundary layer. For example, in the uppermost column of the vertical tank, T32 is the first point where the steep increase occurs, followed by T31, T30, T29, and T28. Also, it can be seen that a stratified temperature distribution occurs from the upper to the lower part of the vertical tank at the final stage of the melting process. As an example, the row identified by the red color has the highest temperature value, followed by the rows identified by blue, green, and black colors. The diminishing of the convection current causes the stratification of temperatures at the upper part of the tanks. Considering the temperature distribution inside the horizontal unfinned tank (Fig. 6 (b)), it can be seen that the temperature at any given row rises almost identically, and the rows closer to the isothermal wall experience the incremental trend sooner. Temperature fluctuation can also be detected when the liquified PCM touches the tip of the thermocouples. Temperature fluctuation is due to the presence of irregular convection cells known as Benard cells in the thin liquid PCM layer. Further, it can be seen that the final temperature values are almost the same regardless of the location of the thermocouples. Also, it is evident that temperature stratification does not occur in the horizontal tanks due to the development of robust vortical and chaotic flows that cause effective mixing and blending of the liquid PCM.

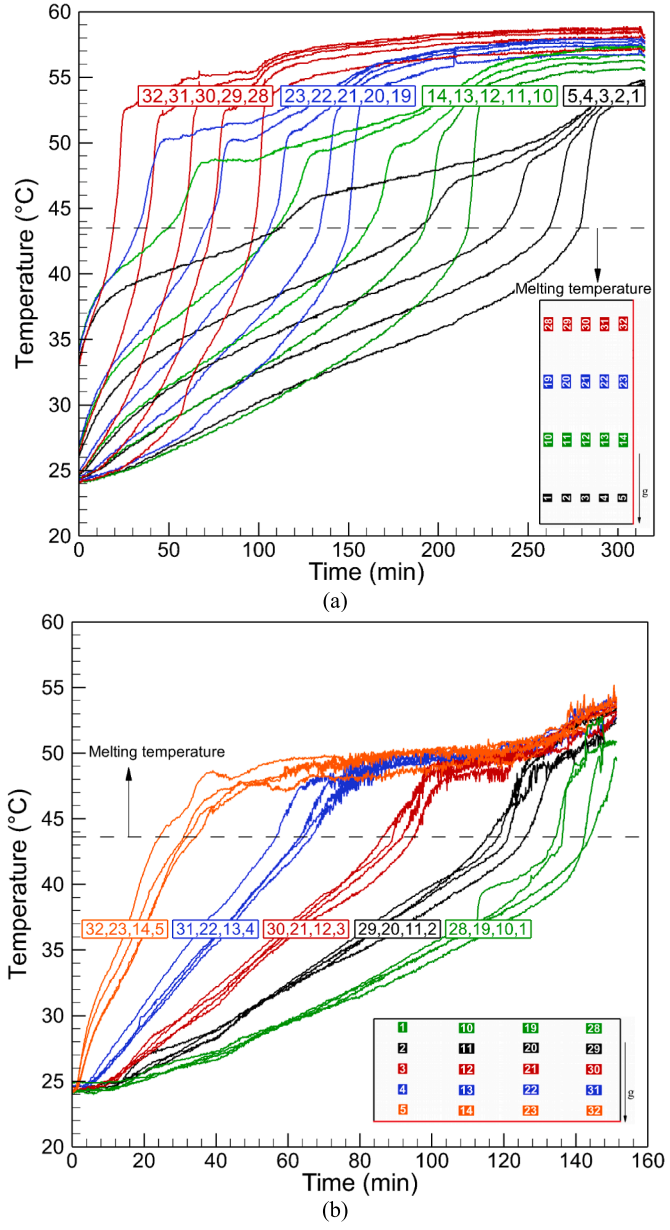

Fig. 6. Temperature variation inside the vertical (a) and horizontal (b) unfinned tanks.

Fig. 7 illustrates the average temperature at different sections of finned enclosures with vertical (a) and horizontal (b) orientations while wall temperature is maintained at 60 °C. Based on the average temperature variation within the vertical tanks (Fig. 7 (a)) and in section-1, it is apparent that the rectangular fin has the highest average temperature, followed by perforated and pin fins. This can be attributed to the higher concentration of rectangular fins at the tank's lower part, primarily driven by the conduction mechanism. Considering section-4, it can be seen that the final average temperature of the pin–fin configuration is a little higher than the two others revealing the presence of more powerful natural convection flows at the upper section of the tank with pin–fin structure. In addition, temperature stratification exists in vertically oriented finned tanks, with section-4 having the highest value, followed by sections 3, 2, and 1. As shown in Fig. 7 (b), section-1 in the horizontal tanks has a higher average temperature than section-3 due to the presence of two fins, while section-3 is confined between one fin and an isolated wall. Consequently, a lateral temperature gradient is evident in a horizontally oriented finned tank with a maximum at the center. The comparison between sections 6 and 8 reveals that section 6 has a higher average temperature, indicating the development of powerful natural convection flows closer to the fins.

4.2. Melt front evolution

A visual representation of melt interface propagation can assist in determining the patterns of natural convection currents and provides useful information regarding the dominant heat transfer mechanism

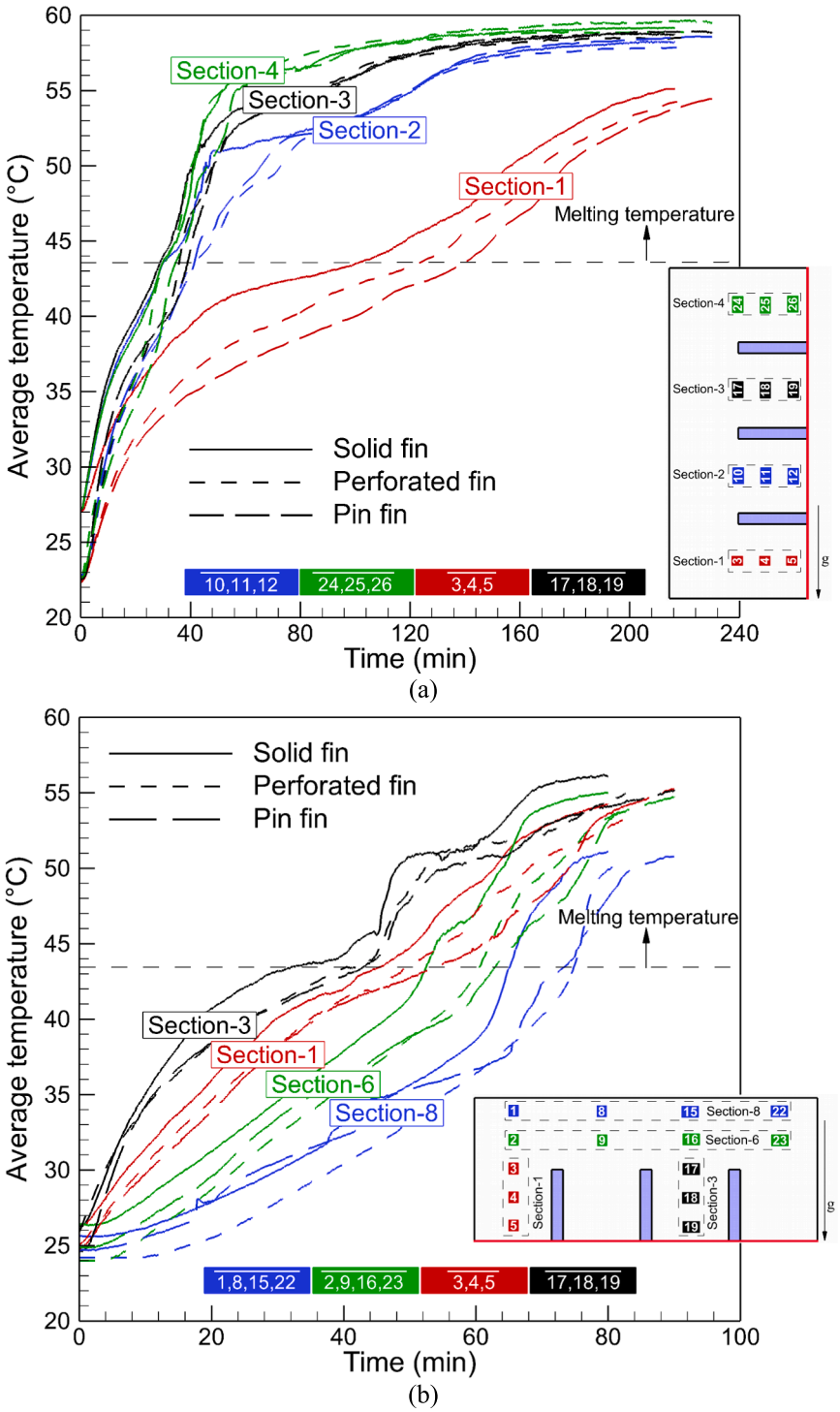

Fig. 7. Average ttemperature variation at different sections of the vertical (a) and horizontal (b) finned tanks.

during the melting process. Fig. 8a depicts the sequential images of the melt front evolution in the finned and unfinned vertical thermal storage tanks at wall temperature of 60℃. Solid and liquid PCM can be identified by the white and black colors, respectively. A high-resolution photography method was used to detect distinctions between the solid and liquid phases clearly. According to Fig. 8a it can be seen that the melting interface moves parallel to the heat transfer surface at the beginning of the phase change process (time instant of 15 min), indicating the dominant role of the conduction mechanism. The limited thermal conductivity of the fin and a temperature gradient along its length result in a greater melting rate at the base of the fin as compared to the tip. It should be noted that a tank with pin–fin configurations has a 3D melting interface, which means that the shape of the melting interface alters along the depth of the tank. However, after liquefying the enclosed PCM between the pin fins, the melting process progresses in a 2D manner. By increasing the thickness of the liquid PCM, the buoyancy force begins to exceed the viscous force, which leads to the establishment of natural convection flow during which the molten PCM absorbs heat from the hot wall and rises upward and descends along the solid–liquid interface. Early in the convection-driven melting process (time

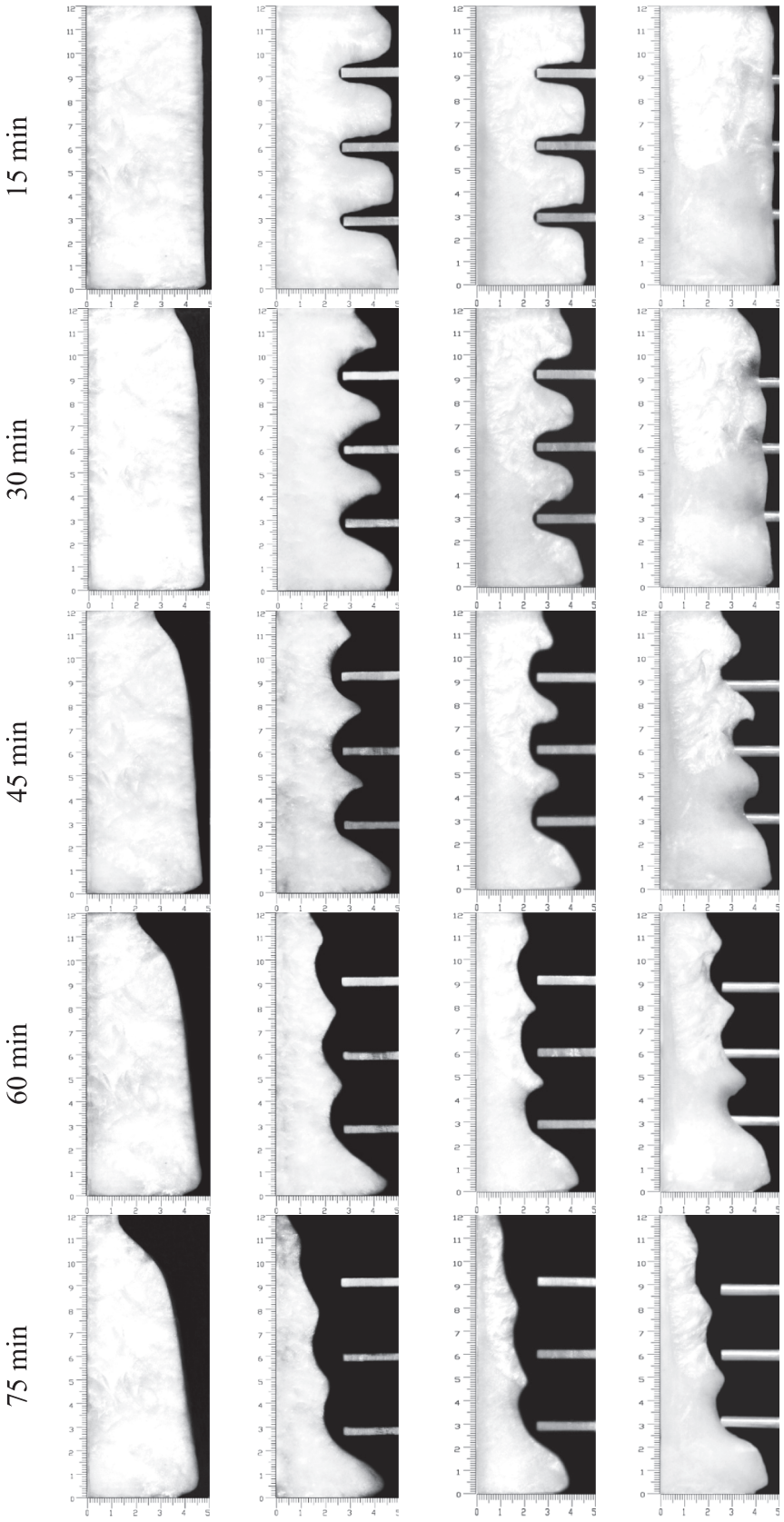

Fig. 8a. Images of the melting process at vertical orientation.

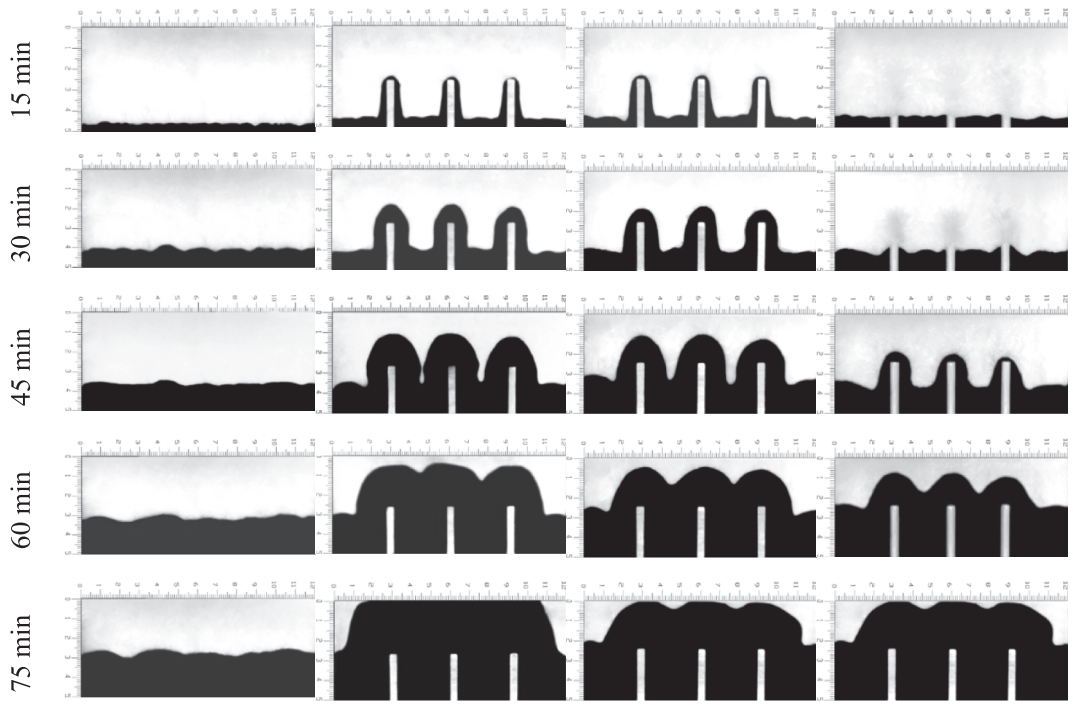

Fig. 8b. Images of the melting process at horizontal orientation.

instant of 30 min), the shape of the melting interface at the half-upper and half-lower sections of the vertical tanks is nearly identical, demonstrating a similar natural convection pattern in both halves. At time instant of 45 min, the amount of liquified PCM is almost identical for rectangular and perforated fin configurations, although it is lower for pin fin configurations. As the melting process continues, this difference diminishes, and nearly the same amount of liquid PCM can be observed in the finned tanks.

Fig. 8b shows the melting process inside the horizontally oriented finned and unfinned tanks. A comparison of the melt front shape between horizontal and vertical tanks indicates that the structure of convection currents in the liquid PCM are totally different when the heating surface is the bottom side of the tank. The wavy shape of the melting interface clearly indicates the establishment of counter-rotating convection cells in horizontal tanks. The concavities along the interface have been caused by a thermal plum between two adjacent counter-rotating convection cells. A plum transports hot liquid bulk from a heated wall to the melting interface, which accelerates the melting process by directly impinging on the interface. As the melting process progresses (time instant of 45 min), the melting rate at the upper section of the vertical tanks increases significantly compared to the lower part. This pattern is more pronounced for pin fin configuration. After being raised from a hot surface, the hot liquid PCM encounters the melting interface and cools down. Thus, the melt interface serves as a cold side during the convection-dominant stage of the melting process. Horizontal tanks have an almost constant length of the melting interface, while vertical tanks have a shrinking size as the melting interface approaches the opposite wall. At the final stage of the melting process (from 60 min onwards), the weakening of convection flows at the upper part of the vertical enclosure due to the shrinkage of the interface results in a lower melting rate at the upper part of the tanks. However, it was observed that the horizontal tanks have a uniform melting rate till the end of the melting process.

4.3. Melt fraction

The impact of adding fins with different configurations on the melting behavior of the PCM can be examined by temporal melt fraction variation, which is determined as the ratio of the liquid PCM volume at each time step to the initial solid PCM volume. Fig. 9 shows the melt fraction variation with time for (a) vertical and (b) horizontal storage tanks at wall temperature of 60°C. It is evident that the higher heat transfer area of the finned tanks improves the melting rate over the unfinned ones. For both vertical and horizontal tanks, it can be seen that the tanks with rectangular fins outperform other fin configurations. In vertical tanks, melt fraction curves initially follow a linear trend and then take the form of bent curve, indicating that the heat transfer rate is decreasing. The heat transfer suppression in vertical tanks can be explained by looking at the growth of the thermal boundary layer over the vertical hot wall. The temperature difference between the wall and liquid PCM decreases from bottom to the top of the tank leading to the lower heat transfer rate form wall to the liquid PCM at the upper level of the tank. However, the melt fraction curves in horizontal tanks follow a nearly constant linear trend until the end of the melting process. In the tanks heated from below, it is noteworthy that the fins are well aligned with the upward natural convection current, thereby ensuring that the heat transfer rate and the strength of the natural convection current are not affected by the growth of the liquid layer and the heated liquid is pushed back from the surface. Similar melting behavior was obtained for the isothermal wall temperatures of 70 and 55°C but are not presented here for the sake of brevity.

4.4. Melting time

Fig. 10 presents the final melting time for the vertical and horizontal finned and unfinned storage tanks at different wall temperatures. It clearly shows that both adding fins and increasing HTF temperature have led to a melting time reduction. Using a horizontally oriented tank with rectangular fins, the PCM melts in 42 min, which is 4 and 7 min shorter than when perforated and pin fins are used. Interestingly, the melting time in unfinned horizontal tanks is less than those of vertical finned tanks. Therefore, it can be concluded that although adding fins can accelerate the melting time, the tank orientation should also be well-selected to minimize the melting time.

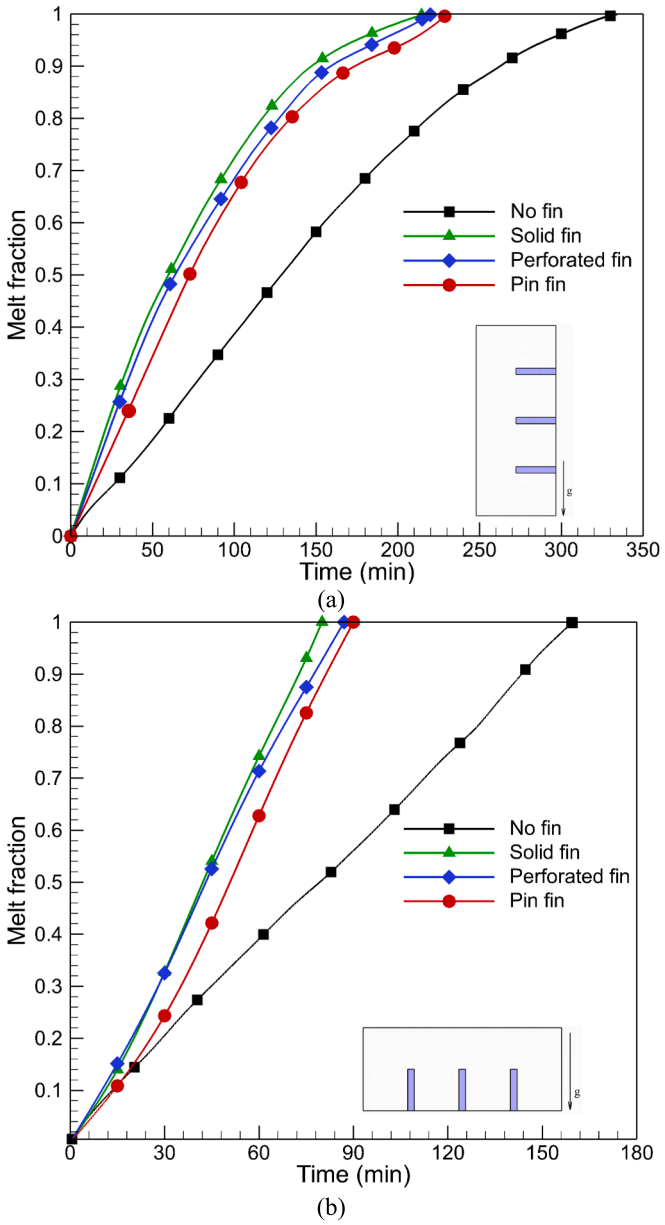

Fig. 9. The melt fraction variation for (a) vertical and (b) horizontal storage tanks.

4.5. Heat transfer characteristics

The melting time reduction (MTR) parameter for different cases is presented in Table. 5 to quantify the effect of parameters such as HTF temperature, fin configuration, and tank orientation on the melting rate of PCM. It has been defined based on the time reduction of each case compared to the unfinned vertical tank at the wall temperature of 55℃. It can be seen that the maximum time reduction at three wall temperatures of 55, 60, and 70℃ belongs to the rectangular fin horizontal storage tank with values of 72.34, 85.05, and 92.15 %, respectively. According to the results, there is no significant difference in melting time between rectangular, perforated, and pin fin tanks at each tank orientation, but there is a considerable difference in fin weight and fin area, which will be discussed in more detail in the following sections.

Fig. 11 shows the time-averaged convection heat transfer coefficient $<\overline{h}>$ and time-averaged heat transfer rate $<\overline{Q}>$ at different wall temperatures and fin configurations normalized by the corresponding values of the unfinned case at a wall temperature of 55℃ (benchmark).

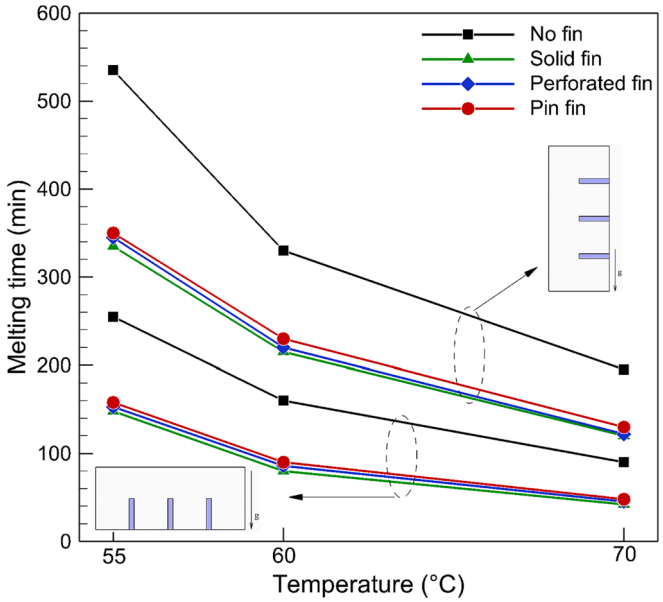

Fig. 10. The complete melting time of each case at different wall temperatures.

Table 5
The MTR values of each case at different wall temperature.

Tank orientation	Fin Type	55℃	60℃	70℃
MTR for vertical tanks (%)	Unfinned	–	38.32	63.55
	Rectangular fin	37.38	59.81	77.57
	Perforated fin	36.45	58.88	77.20
	Pin fin	34.02	57.01	75.70
MTR for horizontal tanks (%)	Unfinned	52.34	70.09	83.18
	Rectangular fin	72.34	85.05	92.15
	Perforated fin	71.03	83.74	91.40
	Pin fin	70.47	83.18	91.03

At the vertically oriented tank Fig. 11 (a), irrespective of wall temperature, the highest value of the heat transfer coefficient belongs to the unfinned tank, followed by pin, perforated and rectangular fin configurations, whereas the trend for the heat transfer rate is the opposite and the rectangular fin case has the highest value. This thermal behavior can be explained by looking at the formation and direction of convection flows in the liquid PCM. For vertical cases, the hindering effect of the horizontal fins against the development of ascending natural convection current along the heated wall decreases the convective heat transfer coefficient. The hampering effect of fins reduces by employing perforated and pin fins among which the pin fins resulted in the best performance. However, it is important to note that the total heat transfer rate is affected by both the convective heat transfer coefficient value and heat transfer area. The increased heat transfer area outperforms the reduced convective heat transfer coefficient resulting in a higher heat transfer rate of the tanks with rectangular fin configuration. Also, it is evident that increasing the wall temperature increases both the heat transfer coefficient and rate parameters as the result of more heat conduction and formation of stronger natural convection currents in the liquid PCM. For the tanks heated from below Fig. 11 (b), the highest heat transfer coefficient value belongs to the pin–fin configuration except at wall temperatures of 55℃ at which the convection current is weak. It should be considered that the convection flow in the horizontal liquid layer is three-dimensional in nature as a result of the establishment of Benard convection cells. Benard convection cells are set up in a planar horizontal layer of liquid PCM heated from below and cooled from above (solid–liquid interface), in which the liquid PCM develops a pattern of lateral convection current known as Benard cells. Employing the rectangular fins interferes with the formation and development of

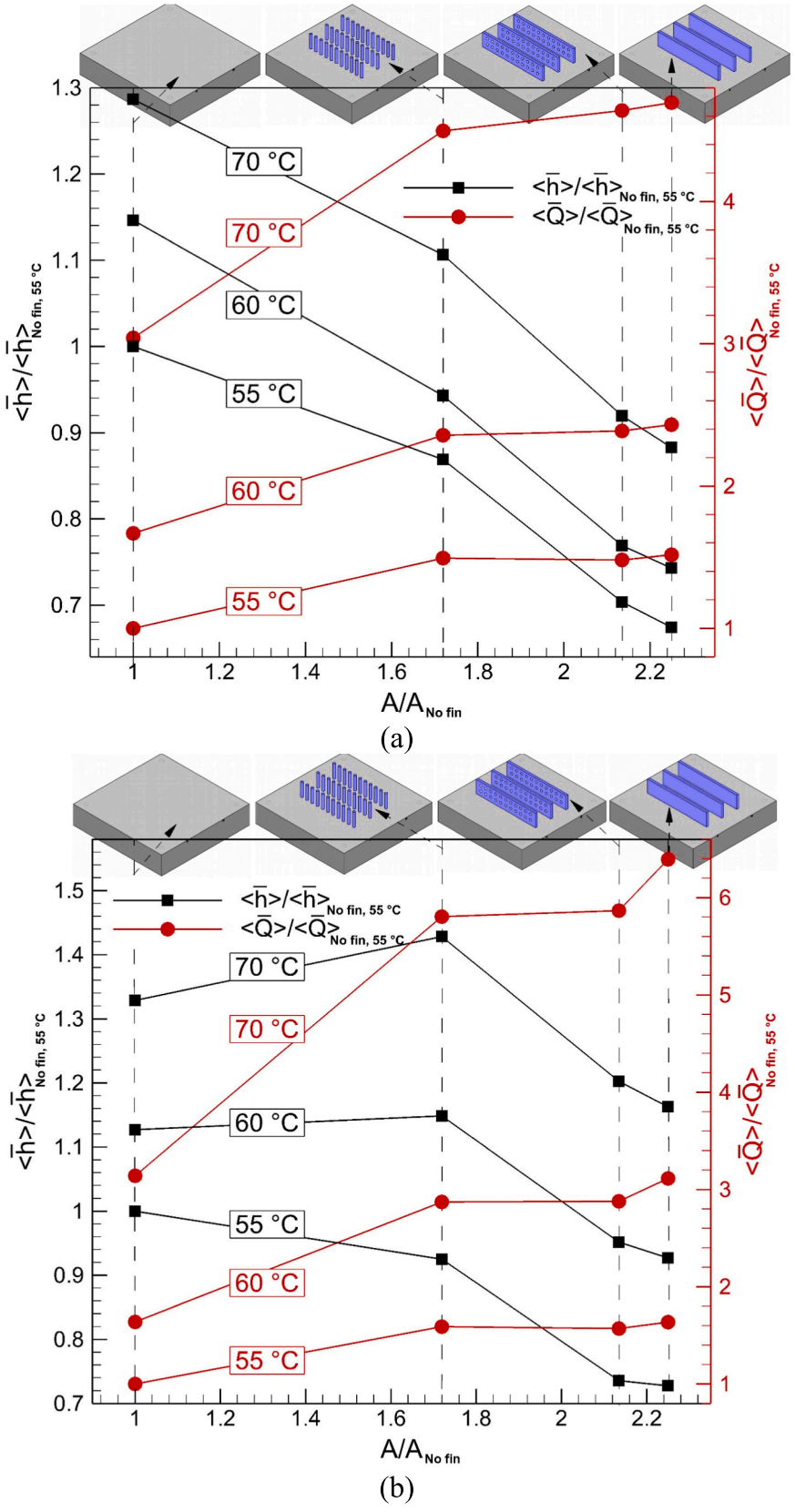

Fig. 11. Normalized $<\bar{h}>$ and $<\bar{Q}>$ values of the (a) vertical and (b) horizontal tanks at different wall temperatures.

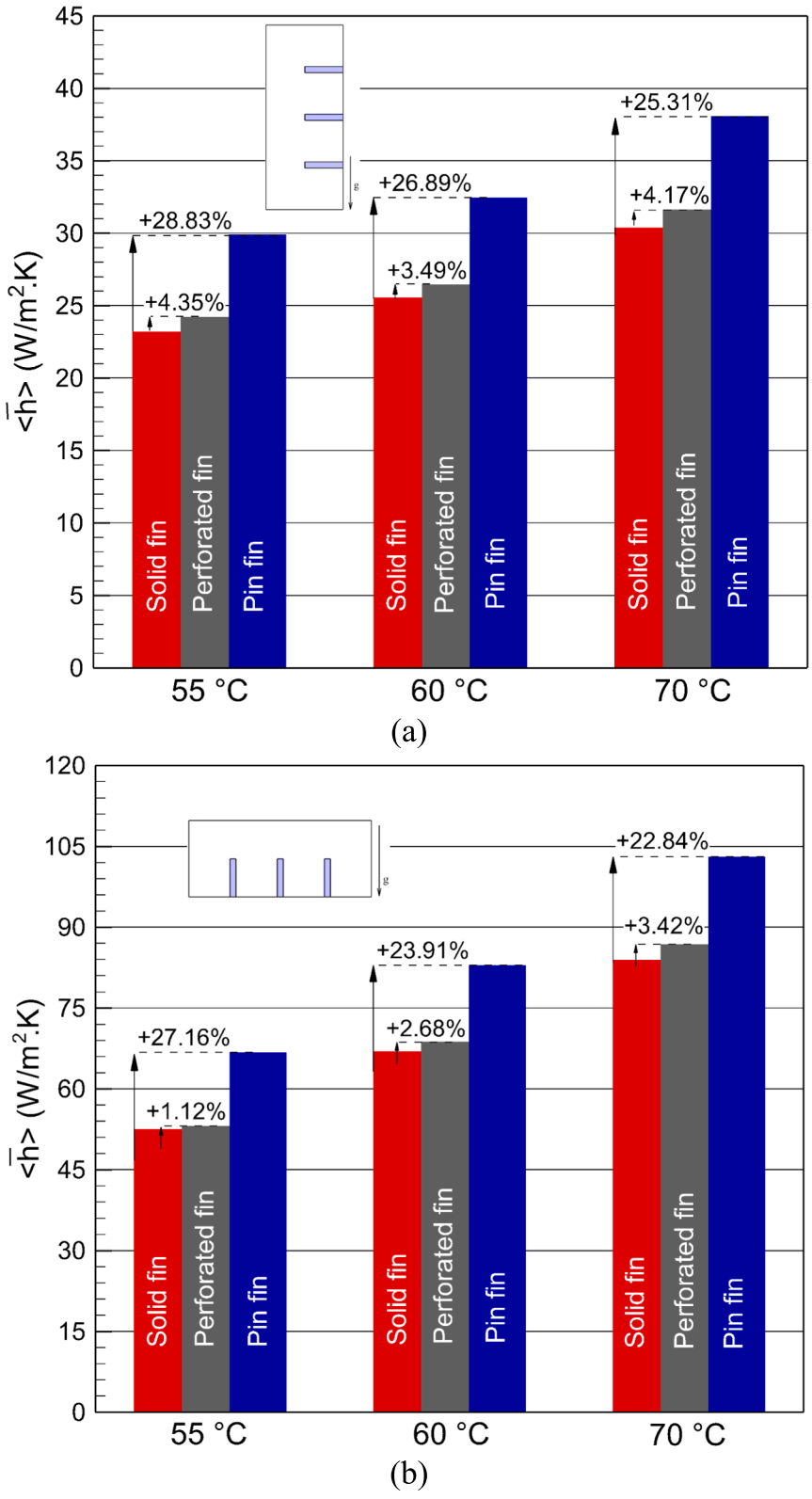

Fig. 12. Comparison of $<\bar{h}>$ value for (a) vertical and (b) horizontal tanks at different wall temperatures.

the Benard Convection cells leading to a decrease in heat transfer coefficient while the perforated fin and pin fin configurations have the less adverse effect on the establishment of the convection cells. It is also seen that the pin fin surface has a higher heat transfer coefficient compared to the plain wall, especially at higher wall temperatures. The results show that by employing pin and perforated fins a higher convection heat transfer coefficient can be achieved compared to the rectangular fins in both horizontal and vertical thermal storage tanks heated from one side. Using this outcome as a guide, a design strategy can be developed for the design of more compact and lighter latent heat storage units at a lower cost.

Fig. 12 quantitively compares the amount of improved time-

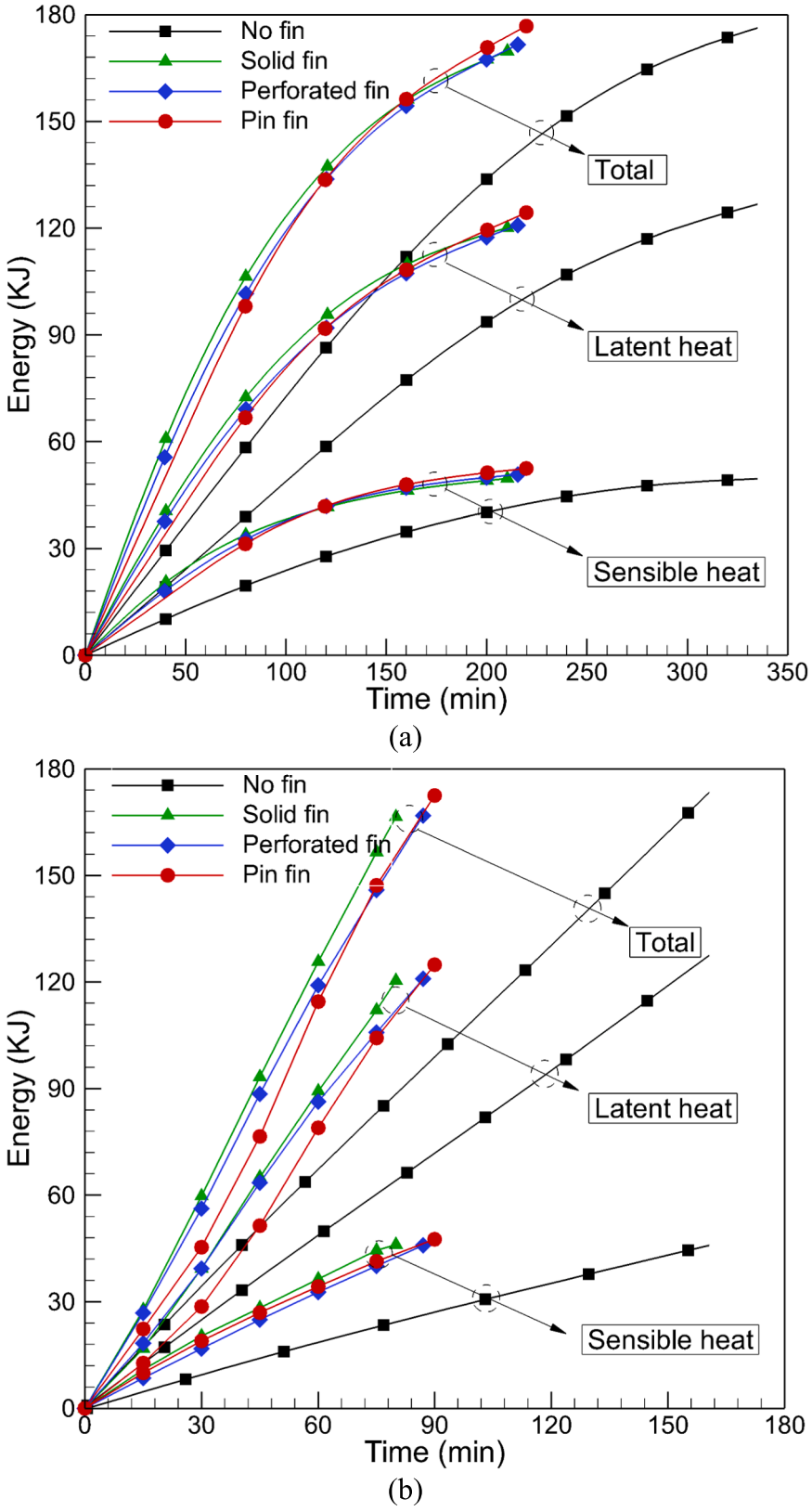

Fig. 13. Variation of the of the stored thermal energy for (a) vertical and (b) horizontal tanks.

averaged heat transfer coefficient (<$\bar{h}$>) in vertical (a) and horizontal (b) orientation at wall temperatures of 55, 60, and 70℃. The highest enhancement value compared to the rectangular fin configuration belongs to the pin fin tank at a wall temperature of 55℃ with values of 28.83 % and 27.16 % for vertical and horizontal orientation, respectively. As mentioned before, the pin fin configuration provides larger space for convection current development, so the <$\bar{h}$> values are much higher than others. The same scenario is also correct for perforated fin

configuration with the difference that in perforated configuration, the space for upward natural convection flows is lower than pin fin configuration. Interestingly, the improvement values for pin fin configuration decrease with an increase in wall temperature. Additionally, it can be seen that the perforated fins exhibit enhanced performance when used horizontally when the wall temperature is raised. Also, it can be concluded that using perforated fin is more effective when they are used at vertical orientation compared to the horizontal orientation.

4.6. Energy storage rate

Fig. 13 shows the storing trend of thermal energy for vertical (a) and horizontal (b) tanks. Three stages can be distinguished in the thermal energy storage process: thermal energy in form of sensible heat in solid PCM from ambient temperature (25 °C) to the melting point (43.5 °C), latent heat at 43.5 °C and sensible heat in liquid PCM from 43.5 °C until melting is complete. The amount of latent heat energy stored in PCM changes proportionally with the amount of melted PCM. Therefore, the similarity between the variation trend of the latent heat and melt fraction depicted in Fig. 9 can be explained. Considering the figures, it is evident that the amount of final thermal energy stored by finned and unfinned tanks is the same. There is no difference in the stored sensible heat and latent heat in the horizontal and vertical orientations (finned and unfinned tanks), but the stored sensible heat in the liquid PCM varies depending on the orientation. Due to the higher average temperature of liquid PCM in vertical tanks, a slightly higher amount of thermal energy has been stored. For the tanks with vertical orientation, the storage rate is curvy with a decreasing trend, whereas for horizontal tanks, it is almost linear till the end. This is due to the long-held dominance of the thermally stratified region in vertical enclosures, while intensive vortical flows in horizontal enclosures postpone the formation of such phenomenon until the very end of melting process. Although the differences in the final stored thermal energy for all configurations are insignificant, a considerable variation in melting time does exist, which highlights the importance of selecting the appropriate fin layout.

5. Conclusion

In this research, the effect of the different fin configurations on the charging rate of PCM in rectangular tanks was examined. Three structures of rectangular, perforated, and pin fins, were fabricated and the performance of the systems was evaluated under different working temperatures and inclination angles. An accurate image processing technique was employed to track the solid–liquid interface and measure the instantaneous melt fractions. The time-averaged heat transfer rates, heat transfer coefficients and energy storage rates were calculated by using melting photographs and temperature recording at different locations of the tanks. According to the study, the following conclusions were drawn:

- Vertical storage tanks experienced gradual melting rate reduction with time due to the shrinkage melt interface and thermal stratification of the melted PCM, while horizontal tanks displayed uniform and faster melting rates throughout the charging process.
- Heat transfer coefficient was improved using pin fins and perforated fins compared to the rectangular fins. This thermal behavior pertains to the facilitation of convection flows through and between the perforated and pin fin structures while the rectangular fins hinder the formation of upward convection flows. The improvement in heat transfer coefficient was more significant using the pin fin structure. The enhancement values for vertical and horizontal orientations of pin fins at a wall temperature of 55 ℃ were 28.8 % and 27.2 %, respectively.
- The heat transfer rate from the rectangular fins is slightly higher than that from the perforated and pin fin structures and consequently, the melting time is lower. The melting time of PCM in the rectangular-finned vertical tank at a wall temperature of 70 ℃ is 3.3 % and 8.3 % less than the melting times achieved by the perforated and pin fins, respectively. This slight improvement in melting time reduction is at the cost of higher fin volume and mass which increase the weight and cost of the storage tanks. The fin volumes of the pin fin and perforated fins, compared to the rectangular fins, are 71 % and 9 % lower, respectively.
- Considering the vertical unfinned tanks at 55 ℃ as the benchmark, the maximum melting time reduction at three wall temperatures of 55, 60, and 70 ℃ was achieved by the rectangular fin horizontal storage tank with corresponding values of 72.3, 85.0, and 92.1 %, respectively.

CRediT authorship contribution statement

Vahid Safari: Data curation, Formal analysis, Investigation, Writing – original draft. **Babak Kamkari:** Investigation, Methodology, Project administration, Supervision, Visualization, Writing – review & editing. **Neil Hewitt:** Supervision, Writing – review & editing. **Kamel Hooman:** Supervision, Writing – review & editing.

Declaration of competing interest

The authors declare that they have no known competing financial interests or personal relationships that could have appeared to influence the work reported in this paper.

Data availability

Data will be made available on request.

References

[1] Y. Grosu, I. Ortega-Fernández, L. González-Fernández, U. Nithiyanantham, Y. F. Baba, A. Al Mers, A. Faik, Natural and by-product materials for thermocline-based thermal energy storage system at CSP plant: Structural and thermophysical properties, Appl. Therm. Eng. 136 (2018) 185–193, https://doi.org/10.1016/J.APPLTHERMALENG.2018.02.087.
[2] J.K. Chen, I.S. Huang, Thermal properties of aluminum–graphite composites by powder metallurgy, Compos. Part B Eng. 44 (2013) 698–703, https://doi.org/10.1016/J.COMPOSITESB.2012.01.083.
[3] W.W. Wang, K. Zhang, L.B. Wang, Y.L. He, Numerical study of the heat charging and discharging characteristics of a shell-and-tube phase change heat storage unit, Appl. Therm. Eng. 58 (2013) 542–553, https://doi.org/10.1016/J.APPLTHERMALENG.2013.04.063.
[4] V. Kapsalis, D. Karamanis, Solar thermal energy storage and heat pumps with phase change materials, Appl. Therm. Eng. 99 (2016) 1212–1224, https://doi.org/10.1016/j.applthermaleng.2016.01.071.
[5] A comprehensive review on pit thermal energy storage: Technical elements, numerical approaches and recent applications, J. Energy Storage. 55 (2022) 105716. doi: 10.1016/J.EST.2022.105716.
[6] M. Sun, T. Liu, H. Sha, M. Li, T. Liu, X. Wang, G. Chen, J. Wang, D. Jiang, A review on thermal energy storage with eutectic phase change materials: Fundamentals and applications, J. Energy Storage. 68 (2023) 107713, https://doi.org/10.1016/j.est.2023.107713.
[7] S. Tan, X. Zhang, Progress of research on phase change energy storage materials in their thermal conductivity, J. Energy Storage. 61 (2023) 106772, https://doi.org/10.1016/j.est.2023.106772.
[8] Z. Chang, K. Wang, X. Wu, G. Lei, Q. Wang, H. Liu, Y. Wang, Q. Zhang, Review on the preparation and performance of paraffin-based phase change microcapsules for heat storage, J. Energy Storage. 46 (2022) 103840, https://doi.org/10.1016/j.est.2021.103840.
[9] M. Mozafari, A. Lee, J. Mohammadpour, Thermal management of single and multiple PCMs based heat sinks for electronics cooling, Therm. Sci. Eng. Prog. 23 (2021) 100919, https://doi.org/10.1016/J.TSEP.2021.100919.
[10] M.A.E. Moghaddam, D.D. Ganji, A comprehensive evaluation of the vertical triplex-tube heat exchanger with PCM, concentrating on flow direction, nanoparticles and multiple PCM implementation, Therm. Sci. Eng. Prog. 26 (2021) 101124, https://doi.org/10.1016/J.TSEP.2021.101124.
[11] X. Zhang, Y. Ren, Y. Ren, Y. Yan, A novel bionic packed bed latent heat storage system filled with encapsulated PCM for thermal energy collection, Therm. Sci. Eng. Prog. 35 (2022) 101449, https://doi.org/10.1016/J.TSEP.2022.101449.
[12] A. Sharma, H.B. Kothadia, S. Singh, B. Mondal, Solidification of nanoparticle-based PCM in a fin-aided triplex-tube energy storage system for cooling applications,

Therm. Sci. Eng. Prog. 42 (2023) 101872, https://doi.org/10.1016/J.TSEP.2023.101872.
[13] M. Nitsas, I.P. Koronaki, Performance analysis of nanoparticles-enhanced PCM: An experimental approach, Therm. Sci. Eng. Prog. 25 (2021) 100963, https://doi.org/10.1016/J.TSEP.2021.100963.
[14] Y. Sheikh, M. Fatih Orhan, M. Kanoglu, Heat transfer enhancement of a bio-based PCM/metal foam composite heat sink, Therm. Sci. Eng. Prog. 36 (2022) 101536, https://doi.org/10.1016/J.TSEP.2022.101536.
[15] Z. Zhou, Z. Hu, D. Wang, H. Wu, Visualized-experimental investigation on the melting performance of PCM in 3D printed metal foam, Therm. Sci. Eng. Prog. 31 (2022) 101298, https://doi.org/10.1016/J.TSEP.2022.101298.
[16] V. Safari, B. Kamkari, M. Zandimagham, N. Hewitt, Transient thermal behavior of a passive heat sink integrated with phase change material: A numerical simulation, Int. J. Thermofluids. 20 (2023) 100454, https://doi.org/10.1016/J.IJFT.2023.100454.
[17] C. Zhao, M. Opolot, M. Liu, J. Wang, F. Bruno, S. Mancin, K. Hooman, Review of analytical studies of melting rate enhancement with fin and/or foam inserts, Appl. Therm. Eng. 207 (2022) 118154, https://doi.org/10.1016/J.APPLTHERMALENG.2022.118154.
[18] I.A. Laasri, Z. Elmaazouzi, A. Outzourhit, M.O. Mghazli, Investigation of different topology-optimized fin structures in a cylindrical latent heat thermal energy storage unit, Therm. Sci. Eng. Prog. 33 (2022) 101372, https://doi.org/10.1016/J.TSEP.2022.101372.
[19] C. Ao, S. Yan, X. Zhao, N. Zhang, Y. Wu, Enhanced heat transfer in a latent heat thermal energy storage unit using a longitudinal fin with different structural parameters, Therm. Sci. Eng. Prog. 43 (2023) 101975, https://doi.org/10.1016/J.TSEP.2023.101975.
[20] N.S. Dhaidan, A.F. Hassan, A.M. Rasheed Al-Gaheeshi, F.N. Al-Mousawi, R. Z. Homod, Experimental investigation of thermal characteristics of phase change material in finned heat exchangers, J. Energy Storage. 71 (2023) 108162, https://doi.org/10.1016/j.est.2023.108162.
[21] S.H. Kim, S.H. Park, S. Pandey, M.Y. Ha, Effects of fin positioning on the thermal performance of a phase change material–filled heat sink with horizontal fins, J. Energy Storage. 68 (2023) 107756, https://doi.org/10.1016/j.est.2023.107756.
[22] B. Kamkari, D. Groulx, Experimental investigation of melting behaviour of phase change material in finned rectangular enclosures under different inclination angles, Exp. Therm. Fluid Sci. 97 (2018) 94–108, https://doi.org/10.1016/j.expthermflusci.2018.04.007.
[23] S. Pourhemmati, S. Hossainpour, Thermal improvement of the vertical plate-fin heat sink by variable fin thickness pattern and utilizing phase change material: A numerical investigation, J. Energy Storage. 59 (2023) 106480, https://doi.org/10.1016/J.EST.2022.106480.
[24] D.K. Kim, Thermal optimization of internally finned tube with variable fin thickness, Appl. Therm. Eng. 102 (2016) 1250–1261, https://doi.org/10.1016/J.APPLTHERMALENG.2016.04.060.
[25] K. Shank, J. Bernat, Q. Justice, P. Niksiar, S. Tiari, Experimental study of a latent heat thermal energy storage system assisted by variable-length radial fins, J. Energy Storage. 68 (2023) 107692, https://doi.org/10.1016/j.est.2023.107692.
[26] C. Nie, S. Deng, J. Liu, Effects of fins arrangement and parameters on the consecutive melting and solidification of PCM in a latent heat storage unit, J. Energy Storage. 29 (2020) 101319, https://doi.org/10.1016/j.est.2020.101319.
[27] P. Rawat, Ashwni, A.F. Sherwani, A numerical study on the impact of fin length arrangement and material on the melting of PCM in a rectangular enclosure, Int. J. Heat Mass Transf. 205 (2023) 123932. doi: 10.1016/J.IJHEATMASSTRANSFER.2023.123932.
[28] L.L. Tian, X. Liu, S. Chen, Z.G. Shen, Effect of fin material on PCM melting in a rectangular enclosure, Appl. Therm. Eng. (2020), https://doi.org/10.1016/j.applthermaleng.2019.114764.
[29] V. Safari, B. Kamkari, H. Abolghasemi, Investigation of the effects of shell geometry and tube eccentricity on thermal energy storage in shell and tube heat exchangers, J. Energy Storage. 52 (2022) 104978, https://doi.org/10.1016/J.EST.2022.104978.
[30] L. Darvishvand, V. Safari, B. Kamkari, M. Alamshenas, M. Afrand, Machine learning-based prediction of transient latent heat thermal storage in finned enclosures using group method of data handling approach: A numerical simulation, Eng. Anal. Bound. Elem. 143 (2022) 61–77, https://doi.org/10.1016/J.ENGANABOUND.2022.06.009.
[31] M.E. Nakhchi, M. Hatami, M. Rahmati, A numerical study on the effects of nanoparticles and stair fins on performance improvement of phase change thermal energy storages, Energy. 215 (2021) 119112, https://doi.org/10.1016/j.energy.2020.119112.
[32] Z. Hu, D. Xue, W. Wang, H. Tian, Q. Yin, Y. Xuan, D. Chen, Numerical investigation of the melting characteristics of spherical-encapsulated phase change materials with composite metal fins, J. Energy Storage. 68 (2023) 107902, https://doi.org/10.1016/j.est.2023.107902.
[33] M.M. Kenisarin, K. Mahkamov, S.C. Costa, I. Makhkamova, Melting and solidification of PCMs inside a spherical capsule: A critical review, J. Energy Storage. 27 (2020) 101082, https://doi.org/10.1016/j.est.2019.101082.
[34] V. Safari, H. Abolghasemi, L. Darvishvand, B. Kamkari, Thermal performance investigation of concentric and eccentric shell and tube heat exchangers with different fin configurations containing phase change material, J. Energy Storage. 37 (2021) 102458, https://doi.org/10.1016/J.EST.2021.102458.
[35] V. Safari, H. Abolghasemi, B. Kamkari, Experimental and numerical investigations of thermal performance enhancement in a latent heat storage heat exchanger using bifurcated and straight fins, Renew. Energy. 174 (2021) 102–121, https://doi.org/10.1016/J.RENENE.2021.04.076.
[36] G. Liu, Z. Du, T. Xiao, J. Guo, L. Lu, X. Yang, K. Hooman, Design and assessments on a hybrid pin fin-metal foam structure towards enhancing melting heat transfer: An experimental study, Int. J. Therm. Sci. 182 (2022) 107809, https://doi.org/10.1016/J.IJTHERMALSCI.2022.107809.
[37] C. Zhao, J. Wang, Y. Sun, S. He, K. Hooman, Fin design optimization to enhance PCM melting rate inside a rectangular enclosure, Appl. Energy. 321 (2022) 119368, https://doi.org/10.1016/J.APENERGY.2022.119368.
[38] R. Karami, B. Kamkari, Experimental investigation of the effect of perforated fins on thermal performance enhancement of vertical shell and tube latent heat energy storage systems, Energy Convers. Manag. 210 (2020) 112679, https://doi.org/10.1016/J.ENCONMAN.2020.112679.
[39] R. Pakrouh, M.J. Hosseini, A.A. Ranjbar, R. Bahrampoury, A numerical method for PCM-based pin fin heat sinks optimization, Energy Convers. Manag. 103 (2015) 542–552, https://doi.org/10.1016/j.enconman.2015.07.003.
[40] A. Arshad, H.M. Ali, M. Ali, S. Manzoor, Thermal performance of phase change material (PCM) based pin-finned heat sinks for electronics devices: Effect of pin thickness and PCM volume fraction, Appl. Therm. Eng. 112 (2017) 143–155, https://doi.org/10.1016/j.applthermaleng.2016.10.090.
[41] C. Reuben Raj, S. Suresh, S. Vasudevan, M. Chandrasekar, V. Kumar Singh, R.R. Bhavsar, Thermal performance of nano-enriched form-stable PCM implanted in a pin finned wall-less heat sink for thermal management application, Energy Convers. Manag. 226 (2020) 113466. doi: 10.1016/J.ENCONMAN.2020.113466.
[42] V. Safari, B. Kamkari, K. Hooman, J.M. Khodadadi, Sensitivity analysis of design parameters for melting process of lauric acid in the vertically and horizontally oriented rectangular thermal storage units, Energy. 255 (2022) 124521, https://doi.org/10.1016/J.ENERGY.2022.124521.
[43] M.E. Nakhchi, J.A. Esfahani, Improving the melting performance of PCM thermal energy storage with novel stepped fins, J. Energy Storage. 30 (2020) 101424, https://doi.org/10.1016/j.est.2020.101424.
[44] H. Shokouhmand, B. Kamkari, Experimental investigation on melting heat transfer characteristics of lauric acid in a rectangular thermal storage unit, Exp. Therm. Fluid Sci. 50 (2013) 201–212, https://doi.org/10.1016/J.EXPTHERMFLUSCI.2013.06.010.
[45] S.J. Kline, F.A. McClintock, Describing uncertainties in single sample experiments, Mech. Eng. 75 (1953) 3–8.